REVIEW

Check for updates

Advances in layer-by-layer processing for efficient and reliable organic solar cells

Amaresh Mishra, ID *[a] Nirmala Niharika Bhuyan, ID [a] Haijun Xu ID [b] and Ganesh D. Sharma ID *[c]

Layer-by-layer (LBL) deposition using solution processing is a promising technique for fabricating organic solar cells (OSCs) with high efficiency and stability. In comparison with bulk-heterojunction (BHJ) structures, in the LBL method, the donor (D) and acceptor (A) materials are deposited sequentially, presenting many distinct advantages including a p–i–n-like configuration (D/D:A/A) that may create well-defined and controllable nanostructures to facilitate charge generation and extraction. This concept is an advisable option to fabricate pseudo-bilayer configurations in the active layer of OSCs. At present, high power conversion efficiencies (PCEs) of over 19% in ternary LBL processed OSCs and 11.97% in the processed module (11.52 cm^2) have been successfully realized, indicating that the selection of an appropriate ternary system is an effective strategy to improve the morphology of the active layer towards efficient and stable OSCs. Moreover, the unique merits of LBL configuration in individual layer processing enable it to be a promising approach for large-scale printing and further commercialization of OSCs. In this article, we summarize the recent advances in LBL OSCs, focusing on the selection of materials, solvents, processing parameters, device architectures, and stability. We also discuss the key strategies used for further improvement of LBL OSCs from the perspectives of structural design, performance, and scalability. Finally, we discuss the current limitations of BHJ devices and the prospect of LBL OSCs as a promising alternative for high-performance and stable OSCs. We also highlight some key research directions that can help enhance the efficiency and stability of LBL OSCs for their potential applications in the future.

[a] School of Chemistry, Sambalpur University, Jyoti Vihar-768019, Sambalpur, India. E-mail: amaresh.mishra@suniv.ac.in

[b] Jiangsu Co-innovation Center of Efficient Processing and Utilization of Forest Resources, Key Laboratory of Forestry Genetics & Biotechnology of Ministry of Education, College of Chemical Engineering, Nanjing Forestry University, Nanjing 210037, P. R. China

[c] Department of Physics, The LNM Institute of Information Technology (Deemed University), Rupa ki Nagal, Jamdoli, Jaipur, Rajasthan-302031, India. E-mail: gdsharma@lnmiit.ac.in

Amaresh Mishra is an Associate Professor at the School of Chemistry, Sambalpur University, India. He received his PhD in 2000 from Sambalpur University. After a postdoctoral stay at the University of South Florida and University of Akron from 1999–2001, he joined TIFR, Mumbai, India as a Visiting Fellow working on organic light emitting diodes. He then moved to the group of Prof. P. Bäuerle, University of Ulm, Germany in 2005, as a Alexander von Humboldt Fellow and continued as a Group Leader of organic solar cell research until 2015. His current research focuses on the design and development of functional organic and hybrid materials for photovoltaic applications.

Amaresh Mishra

Nirmala Niharika Bhuyan is currently pursuing her PhD under the supervision of Dr Amaresh Mishra at the School of Chemistry, Sambalpur University. Her PhD research focus is on the molecule design and synthesis of functional organic molecules for biological and organic solar cell applications.

Nirmala Niharika Bhuyan

1. Introduction

The field of organic solar cells (OSCs) has witnessed remarkable advances in the last 20 years, thanks to the synthesis of novel organic materials and the design of innovative device structures. Currently, OSC technology is close to the performance of inorganic and perovskite solar cells owing to their unique advantages, such as light weight and potential in constructing large area and flexible devices by adopting a low-cost solution processing technique.[1–10] The initial phase of OSC research involved a simple device structure with a single organic semiconductor as the active layer between two electrodes with different work functions, realizing a very low power conversion efficiency (PCE) due to low exciton dissociation.[11] In OSCs, excitons (bound electron–hole pairs) are formed after absorption of suitable photon energy because of the low dielectric constant of organic materials, which hinder direct electron–hole dissociation as opposed to high dielectric inorganic materials. The excitons are localized on the conjugated backbone.[12,13] In 1986, Tang reported the first donor (D)/acceptor (A) vacuum-deposited planer heterojunction (PHJ) OSCs and attained a PCE of around 1%.[14] The performance of PHJ devices was hindered due to the short exciton diffusion length (L_D) of the organic semiconducting materials, which ranged from 5 to 20 nm.[15] This meant that only a small fraction of the excitons generated in the active layer could reach the D:A interface and dissociate into free charges. Hiramoto et al. fabricated three-layered OSCs with a co-deposited interlayer of a D:A mixture between the respective layers, serving as an efficient carrier generation layer.[16,17] In the subsequent year, Sariciftci et al. demonstrated ultrafast photo-induced electron transfer in a conjugated polymer and fullerene (C_{60}) mixture.[18] In 1995, Heeger and co-workers introduced the concept of bulk-heterojunction (BHJ) formed by a mixture of D and A, which facilitated exciton dissociation and charge transport by expanding the D:A interfacial area with a bi-continuous inter-penetrating network leading to an increase of the PCE of OSCs compared to bilayer counterparts (Fig. 1).[19,20]

In the early stage of development, the field of OSCs was focused on a BHJ active layer consisting of fullerene derivatives due to their high electron affinity, ease of accepting electrons, isotropic electron transport, and facilitation of electron delocalization at the donor/acceptor interface.[1,21–25] Many innovations and PCE improvements (ranging from 9 to 11%) were attained using fullerene derivatives as acceptors when paired with a polymer or small molecule as donors.[26–28] However, despite the progress with fullerene based OSCs, it remains challenging to extend the absorption profile to longer wavelengths, modify frontier energy levels, chemical modification of fullerene acceptors, and morphological instability. Moreover, fullerene based OSCs showed high energy losses exceeding 0.8 eV, which reduces the open circuit voltage (V_{OC}).

With the emergence of fullerene-free acceptors (FFAs),[3,5,29] such as ITIC[30] and Y6 derivatives,[31–33] exhibiting extended absorption towards a longer wavelength region which is complementary of the wide/medium bandgap donor, optimization of film morphology, interface engineering, benefit of low energy loss, and device configurations, the PCEs of BHJ OSCs have been improved from ∼3% to 19% in the past 20 years[34–38] and to 20% for tandem solar cells.[39,40] One of the key benefits of these FFAs is that their energy levels (HOMO/LUMO) can be adjusted by careful functionalization, allowing them to absorb in the visible-to-near-IR spectrum, and making them compatible with various donor materials. Also, some recent reports have revealed longer L_D for FFAs compared to fullerenes, allowing an ideal domain size of 20–50 nm for optimized active layers.[41–45] These molecular developments for solution-processed OSCs created new opportunities for their commercialization.[46–51]

A systematic mechanistic approach for photocurrent generation in BHJ OSCs is presented in Fig. 2. The photocurrent generation efficiency (η_e) of OSCs is expressed as $\eta_e = \eta_{abs} \times \eta_{diss} \times \eta_{coll}$, where η_{abs} is the fraction of absorbed photons, η_{diss} is the fraction of dissociated excitons, and η_{coll} is the

Haijun Xu

Haijun Xu attained his PhD at Nanjing University, China (2005), and worked as a postdoc at the same institute (2005–2007). He joined Southeast University as an associate professor in 2007–2009, and after that, he worked as a postdoctoral research fellow at Université Bourgogne Franche-Comté in France under Prof. Claude P. Gros (2009–2011). From 2011, he took his current position at Nanjing Forestry University, China. His research interests include synthetic chemistry, organic solar cells, and photophysics.

Ganesh D. Sharma

Ganesh D. Sharma has been working as a Senior Professor of Physics, Electronics Communication and Engineering and Dean (Research and development) at The LNM Institute of Information Technology, Jaipur (Raj.), India, since December 2015. He obtained his PhD degree from the Indian Institute of Technology, New Delhi in 1985 and then joined JNV University, Jodhpur (Raj.), India, as an Assistant Professor and subsequently as a Professor. His area of research is organic solar cells, nanocrystalline organic–inorganic hybrid solar cells, fuel cells, and organic nanomaterials for energy conversion. He has published more than 330 research papers.

Fig. 1 Schematic representation of the preparation of BHJ and LBL OSCs.
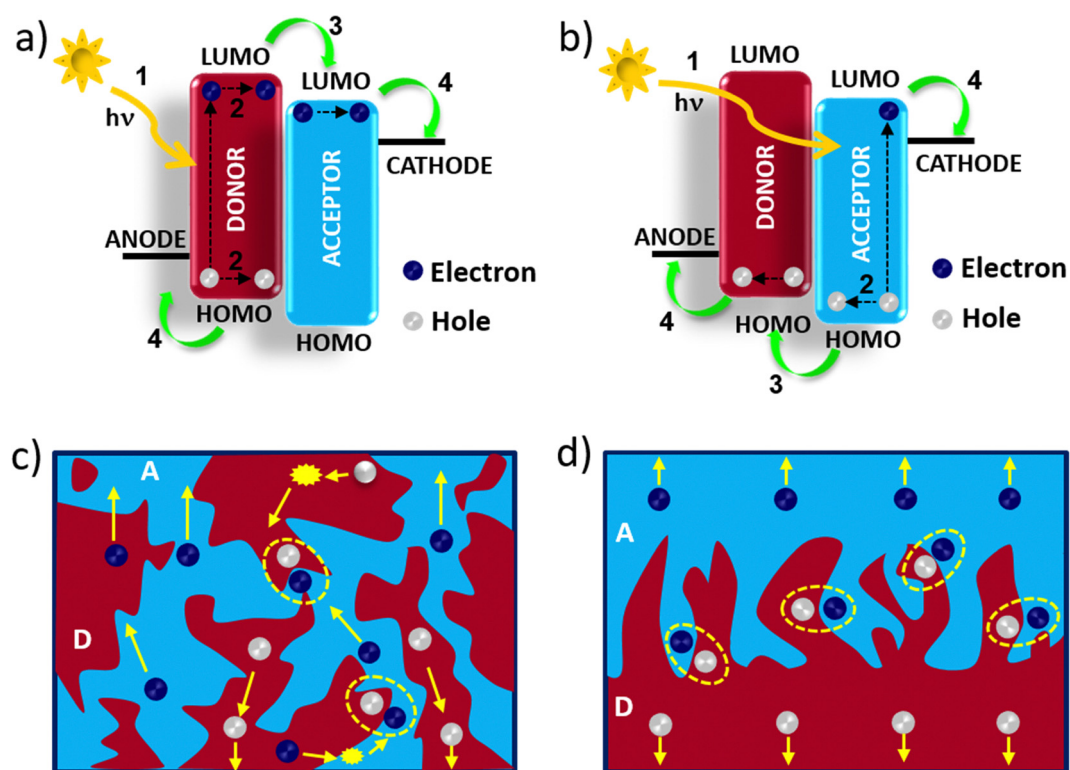

Fig. 2 Fundamental mechanistic approach for photocurrent generation in D−A heterojunction OSCs showing (a) excitation of the donor, and (b) excitation of the acceptor; (1) absorption of photons to generate excitons (bound electron–hole pairs) in both D and A; (2) exciton diffusion to the D/A interface within its lifetime and diffusion length; (3) exciton separation at the D/A interfaces where the e$^-$ jumps to the acceptor and h$^+$ stays in the donor; (4) transport and collection of e$^-$ and h$^+$ at the cathode and anode, respectively. Charge separation and charge transport process at the D/A interface in (c) bulk-heterojunction (BHJ) and (d) layer-by-layer (LBL) OSCs.

efficiency of charge collection by the electrode after the exciton dissociation and is influenced by the internal electric field and optimal morphology in the vertical direction. The optimization of BHJ morphology depends on various processing conditions, such as the D:A weight ratio, the solvent used for processing, co-solvent, additive treatment, interfacial modifications, thermal/solvent annealing, aggregation in the blend, crystallinity, and miscibility of the D and A phase.[52–58] One of the challenges in BHJs is to achieve a balanced and optimal D/A phase separation along the vertical direction, which leads to increased bimolecular recombination and reduced charge extraction.[59–62] The quality of the interpenetrating network in BHJ films strongly depends on the mixing of the D:A components and the choice of solvent for processing. Therefore, developing strategies to

optimize the vertical phase separation along with enriched D/A domains near the respective electrodes is essential to improve the η_{coll} of BHJ solar cells.[63]

Compared to BHJs, the quasi-planar (also called the pseudo-bilayer) heterojunction OSCs processed by a layer-by-layer (LBL) deposition or sequential deposition technique have several advantages and could be cost-effective (Fig. 1).[64–67] The LBL method can avoid the complex nanometer-scale morphology obtained in the BHJ structure and do not depend on the material composition for processing. The approach of the LBL technique using sequential deposition of D and A layers is a viable option to achieve p–i–n type D/(D:A)/A pseudo-bilayer configuration. FFAs with diverse molecular geometries can overcome the drawbacks of fullerene-based acceptors, and together with LBL-processing both the PCE and the stability of the devices can be enhanced.[68,69] The formation of vertical phase separation through LBL-processing is not only beneficial for exciton separation but also offers channels for charge carrier transport and collection and thereby suppressing the charge recombination in the device. Various processing techniques, such as spin-coating, doctor blade coating and slot-die coating, are used to prepare LBL thin films. Moreover, each technique requires careful control of certain parameters that affect the coating properties. These parameters include the solution concentration, solvent, viscosity, temperature, substrate speed, and drying time. One of the advantages of LBL deposition over BHJs is that it allows each layer to be processed independently, which can facilitate large-scale printing for commercial applications. However, sequential processing faces a challenge of balancing exciton dissociation and charge collection, which are affected by the layer distribution and vertical

phase separation. To address this challenge, various methods have been employed, such as the use of orthogonal solvents and co-solvents, applying additives, and annealing of the active layer to optimize the morphology and OSC performance. Friend and Hou groups independently reported a significant breakthrough in the progress of FFA-based LBL OSCs.[70,71] OSCs based on LBL-processing were then investigated by many research groups using a variety of D/A materials to optimize the vertical phase separation, and device engineering. The rapid growth of research on LBL OSCs is evidenced by the remarkable surge of publications in the last 5 years reaching PCEs over 19%,[72–77] which is on par with the BHJ OSCs with improved stability (Fig. 3). Nevertheless, the emergence of new materials and fabrication techniques has stimulated the development of LBL approaches in recent years and opened possibilities for the fabrication of large area devices.

The LBL blade coating technique also enabled the preparation of large area solar modules (3.3 cm^2 and 11.52 cm^2) with high PCEs of 13.88% and 11.86%, respectively.[78] These PCEs are difficult to achieve using a BHJ structure. Therefore, the solution-processed LBL deposition method may be more effective to fabricate stable and reproducible high performance OSCs, specifically for printing roll-to-roll large-area devices.[79]

In this review, we aim to provide a comprehensive overview of the recent advances and challenges in solution processed LBL OSCs, covering new materials development to processing conditions and device architecture aspects and emphasizing their advantage over BHJ structures. We discuss the progress made in LBL OSCs from laboratory scale to large area fabrications and highlight the future directions for this field. The most recent citations are covered until August 2023. This review
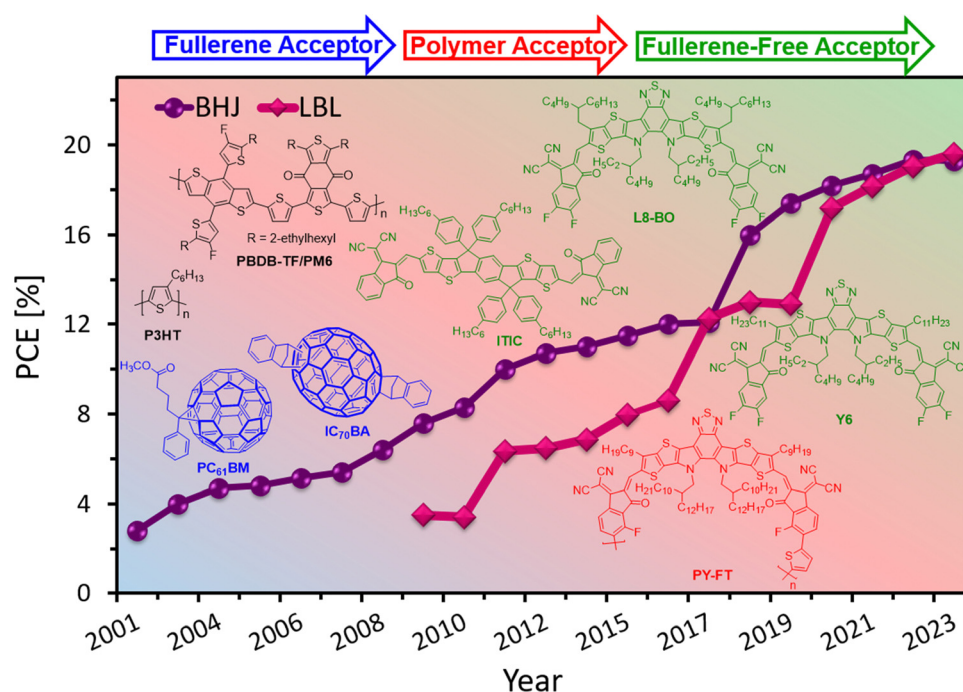

Fig. 3 The PCE development for BHJ and LBL OSCs over previous years.

includes 198 citations, of which ∼100 citations are from 2021 to 2023 showing the story of this dynamic development. The donor materials used in these studies are presented in Fig. 4 and 5.

2. Working principle of BHJ and LBL-processed OSCs

It is established that the PCE of OSCs is directly associated with the BHJ active layer morphology. The domain size of both the donor and acceptor in the active layer must be balanced. For larger domain sizes the excitons will be lost before reaching the D/A interface and hamper the exciton dissociation efficiency. For the efficient transport of charge carriers toward the electrodes, a bi-continuous interpenetrating network is required, otherwise, the charge carriers will be lost due to the excessive charge recombination and thereby reducing the OSCs performance.[80,81] In BHJ OSCs it is very difficult to control the nanoscale morphology as it is very sensitive to the material structure and processing conditions such as the D to A weight ratio and post-treatment conditions. Controlling and predicting the BHJ morphology, which depends on the processing conditions, is also a challenge as the solution process of the mixture of D and A materials led to complicated dynamics and kinetics during the morphological evolution. Since the BHJ morphology is not a thermodynamically stable state, there is a decrease in the stability of OSCs owing to the change in morphology during the device operation. Therefore, the concept of LBL processing using a sequential deposition technique was developed to overcome the above-mentioned limitations of BHJ based OSCs. In LBL-processed OSCs, the choice of solvents and co-solvents is very crucial which regulate the interdiffusion of D and A layers to realize suitable p–i–n structures. During the deposition of the top layer, the bottom layer should not be completely dissolved. Therefore, the D and A materials are dissolved in orthogonal or even semi-orthogonal solvents to avoid washing of the bottom layer. The lower and upper layers are dispersed by swelling or wetting of the solvent forming an intermixed-BHJ interlayer. The addition of solvent or solid additives is another approach by which the interdiffusion of D and A molecules can be enhanced and fine-tune the morphology of the quasi-planar heterojunction. The morphology of the LBL processed active layer has the advantage of both the planar and BHJ structures in which the BHJ layer is sandwiched between the planar layers. The exciton dissociation and charge transport are facilitated by the vertical structure formation.[82] Therefore, the exciton dissociation and charge collection efficiencies are increased in LBL OSCs, which can improve the device performance. The thickness and crystallinity of each layer can be controlled separately in the LBL method, thereby simplifying the optimization process for the device preparation compared with BHJ counterparts, which is beneficial for roll-to roll printing. By adjusting the thickness of the active layer, the transmittance of semitransparent organic solar cells can be enhanced. Moreover, the LBL processed active layers attained a

thermodynamically stable state, which is beneficial for improving the long-term stability of OSCs.

3. Development of LBL processed OSCs

In this section, we discuss the OSCs prepared using a sequential/LBL deposition technique and its advantage over the traditional BHJ devices prepared from D:A blends. The LBL deposition has the advantage of forming independent D/A layers close to the cathode/anode, respectively, for better charge transport. At the same time, a BHJ interlayer is formed by swelling during deposition of the top layer which has the advantage of forming vertical morphology. The structures of fullerene derivatives are shown in Fig. 6 and the additives used are depicted in Fig. 7.

3.1. LBL-processed binary OSCs with fullerene-based acceptors

In 2009, Wang *et al.* for the first time constructed an LBL-processed OSC using a P3HT/PC$_{61}$BM blend and the resulting device displayed an enhanced photocurrent compared to those in the corresponding BHJ counterpart.[83] Schwartz and co-workers fabricated bilayer P3HT/PC$_{61}$BM-based LBL OSCs using *o*-dichlorobenzene (*o*-DCB) and dichloromethane (DCM) as orthogonal solvents and achieved a PCE of 3.5% (Table 1).[84] The thickness of the P3HT layer was 140 nm, while the PC$_{61}$BM layer was only 34 nm thick. They observed that the geometry of the LBL OSC is much simpler than the BHJ devices, which has a complex nanometer-scale morphology. The quality of the interpenetrating network in BHJ devices depends significantly on how well the two components are mixed in the blend film, which is affected by the processing conditions. The fluorescence quenching study showed efficient exciton splitting in the bilayer independent of the film thickness of P3HT. Wong *et al.* confirmed that the LBL method can attain a better PCE when the P3HT layer is produced by rapid evaporation from a processing solvent.[85] The rapid evaporation process reduced the packing of the P3HT layer, which is expected to promote the diffusion of PC$_{61}$BM into the P3HT layer to form the desired BHJ interlayer. Lin *et al.* reported that the PCE of the P3HT/PC$_{61}$BM-based LBL OSCs depends upon the thickness of the PC$_{61}$BM layer and morphology of the BHJ created in the LBL film which is suitable for reducing the charge recombination.[86] Loiudice *et al.* reported a PCE of 3.45% for LBL-processed OSCs based on P3HT/PC$_{61}$BM which was higher than the P3HT:PC$_{61}$BM BHJ counterpart (3.05%)[87] and observed that the vertical phase separation improved the charge percolation/extraction pathways which was responsible for the enhanced PCE. Zhang, *et al.* investigated the effect of crystallinity in LBL-processed and BHJ cast P3HT/PC$_{61}$BM active layers and found that the LBL-processed film showed better morphology and attained a higher PCE of 2.97%.[88] The influence of thermal annealing on the crystallinity of P3HT and PC$_{61}$BM has been investigated by grazing incidence wide-angle X-ray scattering. In the LBL device the reduced regioregularity of P3HT films
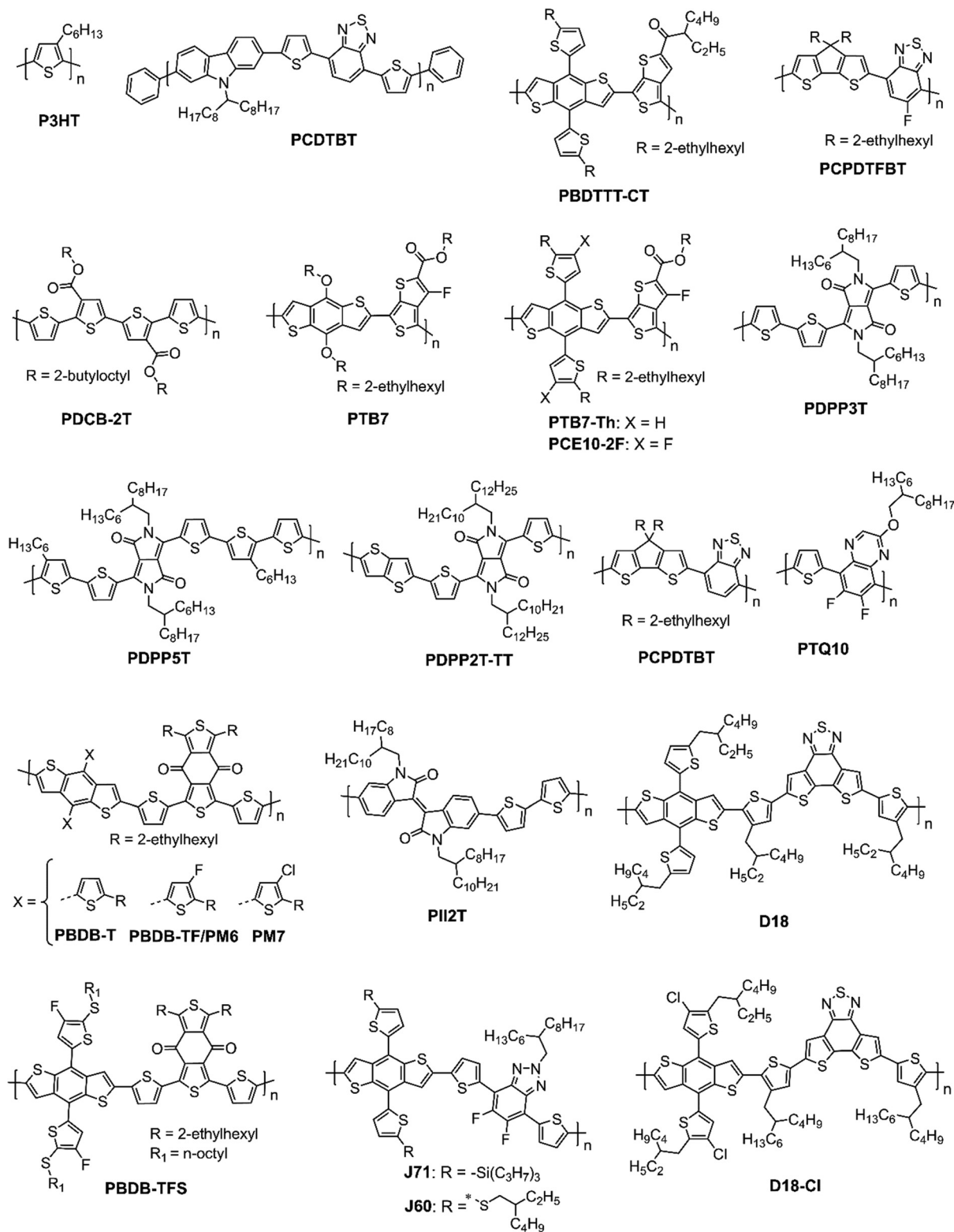
Fig. 4   Chemical structure of polymer donors.

possessed extra amorphous regions allowing the growth of $PC_{61}BM$ crystallites which were helpful for enhanced performance. However, in the BHJ device the best performance was obtained when the regioregularity of P3HT increased.

Wang et al. fabricated $P3HT/IC_{60}BA$-based LBL OSCs and after careful optimization of the D/A layer thickness and thermal annealing treatment, the resultant OSCs demonstrated a PCE of 5.12% with a high V_{OC} of 0.89 V and FF of 0.70.[89] They further

Fig. 5   Chemical structure of polymer and small molecule donors.

Fig. 6   Chemical structures of fullerene derivatives.

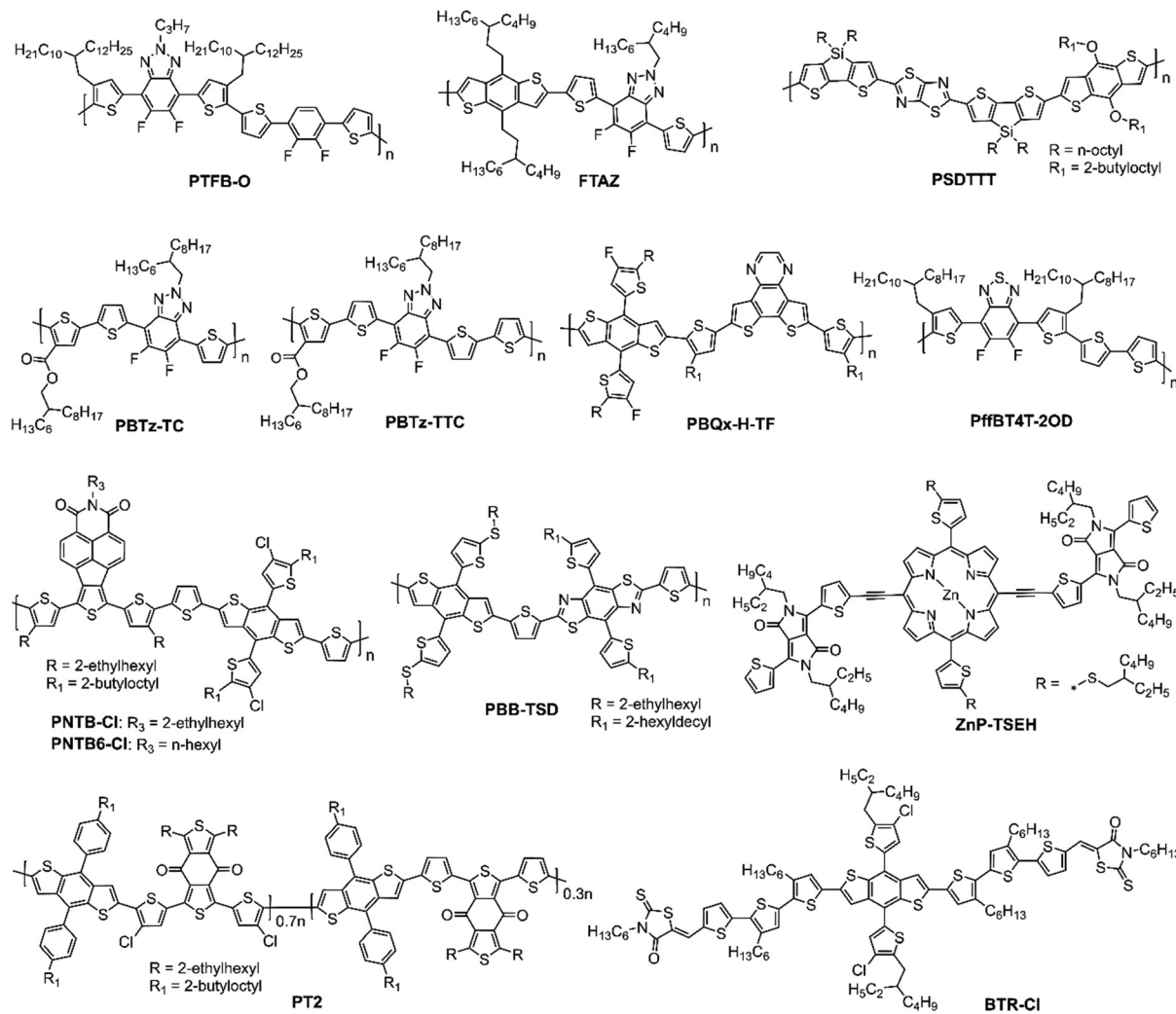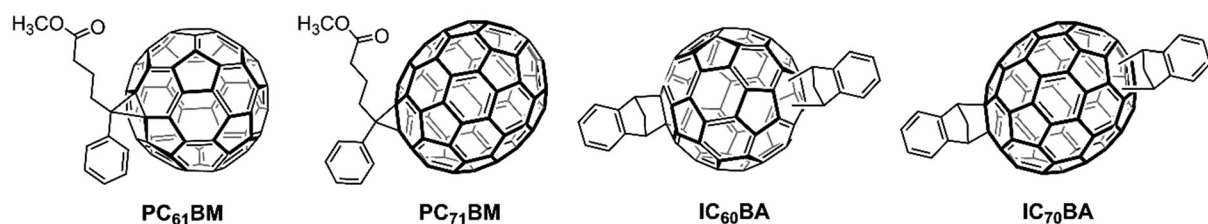improved the PCE to 6.48% using an $IC_{70}BA$ acceptor with a high-lying LUMO energy level.[90]

The Heeger group fabricated LBL-processed OSCs using a PCDTBT/$PC_{71}BM$ blend, in which PCDTBT was dissolved in a mixed solvent system (o-DCB/chlorobenzene, CB), and $PC_{71}BM$ was dissolved in DCM with a little of the above mixed solvent and achieved a PCE of 5.3%.[91] When $PC_{71}BM$ was spin-coated on the top of PCDTBT, it diffused into a PCDTBT film to form the BHJ and exhibited similar domain sizes in the active layer as observed in the conventional BHJ counterpart. Zhan and

co-workers achieved a significantly higher PCE of 7.13% for the PBDTTT-CT/$PC_{61}BM$ based LBL OSCs in contrast to 4.49% for the BHJ counterpart. This improvement was mainly ascribed to the formation of an ideal vertical structure, beneficial for charge transport and collections.[92] Lang et al. explored the fabrication of inverted OSCs using LBL processing, where they have first spin-coated the PCPDTFBT polymer from an o-xylene (o-XY) solution at 90 °C followed by deposition of the $PC_{71}BM$ layer using a mixture of o-XY and o-DCB (4 : 1) as a co-solvent. The LBL OSCs achieved a PCE of 5.84%, slightly higher than the BHJ counterpart (5.35%).[93]
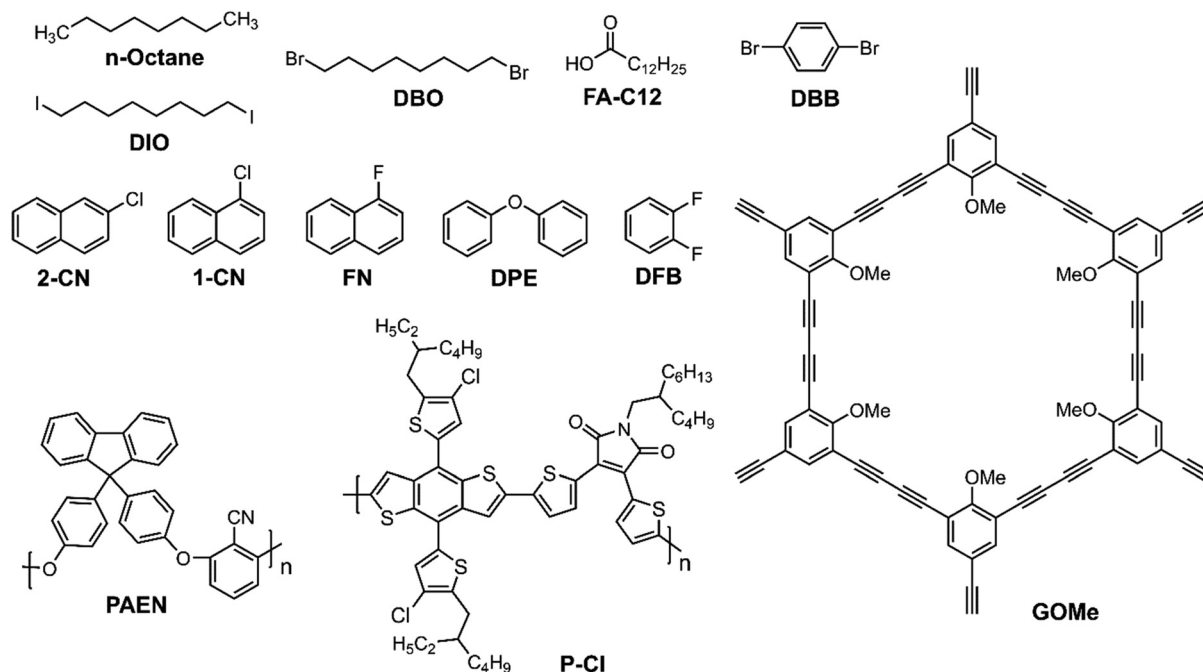
Fig. 7 Chemical structures of solvent- and solid-additives.

Schwartz and co-workers used the Flory–Huggins interaction parameters (χ) to identify the suitable solvent and co-solvents for processing of $PC_{61}BM$ over the polymer donor film.[94] They chose three polymers, PTB7, PSDTTT, and P3HT as the donors along with $PC_{61}BM$ as the acceptor. The polymer layers were spin-coated from CB. The $PC_{61}BM$ was dissolved in 2-chloro-phenol (2-CP) and a suitable co-solvent which can not disturb the bottom polymer layer. The PTB7/$PC_{61}BM$ device gave a PCE of 6.0% when the top layer was processed from 2-CP:1-BuOH. For the amorphous PSDTTT/$PC_{61}BM$ device, 2-CP:isopropyl alcohol (IPA) was chosen for $PC_{61}BM$ deposition to maintain the χ value ~ 1.5 and gave a PCE of 3.8%. The PCE for the LBL devices were slightly higher than the conventional BHJ devices. For P3HT/$PC_{61}BM$, 2-CP:toluene was chosen for the top layer solvent (1.4%).

Theoretically, the ideal LBL-processed OSCs can be fabricated by controlling the extent of swelling and diffusion of one material into another which further depends upon the type of solvents used for the thin film preparation. The formation of the p–i–n structure strongly depends on the solvent used to deposit the top layer. At the same time the swelling of the bottom layer is equally important to regulate the film morphology. Liu et al. used four solvents with different boiling points (o-XY, toluene, CB, o-DCB) to dissolve $PC_{71}BM$ and then applied it over a DPP-based polymer donor (PDPP4T) layer to study how the solvent affects the swelling of the underlying donor film.[95] The OSC displayed an enhanced J_{SC} and FF for the high boiling solvent o-DCB, attaining a PCE of 7.59%. The solvent swelling method formed a trilayer morphology with a D:A interpenetrated layer sandwiched between the lower donor and top acceptor layers. The Janssen group investigated the influence of solvent that dissolves $PC_{71}BM$ on the swelling of the bottom

donor polymer (PDPP5T) layer.[96] They observed that while swelling of the donor layer using a second layer solvent is necessary for sequential processing, the solubility of the acceptor ($PC_{71}BM$) in that particular solvent is equally important for the OSC performance. Using toluene, m-XY, o-XY and 1,2,4-trimethylbenzene (TMB) as the solvent of choice for the upper layer coating, the devices attained PCEs of 0.1%, 0.5%, 3.2% and 5.3%, respectively. The striking difference in the device performance is mostly related to the morphology evolution as studied by scanning electron microscopy (SEM) and atomic force microscopy (AFM). The toluene and m-XY processed active layer showed large crystallites on the surface, while o-XY and TMB-processed layers showed homogeneous distribution of the D:A phase. These results clearly showed the importance of top layer solvent for the formation of an appropriate BHJ interlayer.

It is well known that in LBL deposition, the crystallization in the thin film is associated with the charge carrier transport, and the precise control of the bottom layer crystallinity is crucial for the performance improvement of OSCs. In this respect, Bao et al. selected PII2T as the donor and $PC_{71}BM$ as the acceptor by dissolving $PC_{71}BM$ in different solvents (o-DCB, CB, DCM).[97] The polymer was first deposited by spin-coating and then the dropping of $PC_{71}BM$ for interdiffusion followed by spin-coating and drying to obtain the desired morphology. The device was completed by evaporation of LiF/Al (Fig. 8). When ODCB was used instead of CB for dissolving $PC_{71}BM$, the PCE of LBL OSCs increased from 2.83% to 5.02%. The improved PCE was attributed to the change in the alignment of donor crystallite from edge-on to random state that enhanced the charge transport in the vertical direction and reduced the bimolecular recombination. The results suggested that tuning of the processing solvents to deposit an electron acceptor in

Table 1 Solar cell data for BHJ and LBL-processed OSCs with fullerene-based acceptors

Active layer	Processing method	V_{OC} [V]	J_{SC} [mA cm^{-2}]	FF	PCE [%]	Ref.
P3HT/PC$_{61}$BM	LBL	0.63	8.20	0.66	3.50	84
P3HT/PC$_{61}$BM	LBL	0.64	7.68	0.68	3.39	85
P3HT/PC$_{61}$BM	LBL	0.62	8.92	0.63	3.54	86
P3HT:PC$_{61}$BM	BHJ	0.66	8.67	0.65	3.75	
P3HT:PC$_{61}$BM	LBL	0.60	8.11	0.71	3.45	87
P3HT:PC$_{61}$BM	BHJ	0.59	7.84	0.66	3.07	
P3HT/PC$_{61}$BM	LBL	0.64	8.21	0.57	2.97	88
P3HT:PC$_{61}$BM	BHJ	0.64	6.68	0.42	1.79	
P3HT/IC$_{60}$BA	LBL	0.89	8.21	0.70	5.12	89
P3HT/IC$_{70}$BA	LBL	0.87	10.34	0.71	6.48	90
P3HT/IC$_{70}$BA	BHJ	0.86	10.13	0.71	6.29	
PCDTBT/PC$_{71}$BM	LBL	0.90	10.74	0.66	6.34	91
PCDTBT:PC$_{71}$BM	BHJ	0.87	10.60	0.68	6.26	
PBDTTT-C-T/PC$_{61}$BM	LBL	0.83	15.00	0.55	7.13	92
PBDTTT-C-T:PC$_{61}$BM	BHJ	0.84	9.53	0.54	4.49	
PCPDTFBT/PC$_{71}$BM	LBL	0.71	16.40	0.50	5.84	93
PCPDTFBT:PC$_{71}$BM	BHJ	0.74	15.50	0.47	5.35	
PTB7/PC$_{61}$BM	LBL	0.76	13.70	0.57	6.00	94
PSDTTT/PC$_{61}$BM	LBL	0.73	9.50	0.54	3.80	
P3HT/PC$_{61}$BM	LBL	0.50	6.40	0.45	1.40	
PDPP/PC$_{71}$BM	LBL	0.61	17.95	0.69	7.59	95
PDPP5T/PC$_{70}$BM	LBL	0.57	15.10	0.61	5.30	96
PII2T/PC$_{71}$BM	LBL	0.84	−9.98	0.56	5.02	97
PTB7-Th/PC$_{71}$BM	LBL	0.81	16.60	0.62	8.60	99
PTB7-Th:PC$_{71}$BM	BHJ	0.76	15.80	0.68	8.50	
PCDTBT/PC$_{71}$BM	LBL	0.82	9.87	0.62	5.03	100
PCDTBT:PC$_{71}$BM	BHJ	0.85	9.23	0.51	4.00	
PTB7/PC$_{71}$BM	LBL	0.76	14.80	0.65	7.43	101
PTB7:PC$_{71}$BM	BHJ	0.76	14.70	0.64	7.17	
PCPDTBT/PC$_{71}$BM	LBL	0.63	10.66	0.49	3.36	102
PCPDTBT:PC$_{71}$BM	BHJ	0.62	11.88	0.52	3.87	
PffBT-3/PC$_{71}$BM	LBL	0.66	20.07	0.66	8.70	103
PffBT-3:PC$_{71}$BM	BHJ	0.67	17.75	0.61	7.26	

LBL OSCs is a viable way to adjust the blend film morphology. Shimata *et al.* studied the impact of polymer orientation on the charge dynamics of PCPDTBT/PC$_{61}$BM LBL-OSCs.[98] The charge carrier dynamics at a face-on rich or edge-on interface were controlled *via* side chain modifications. The charge separation was more efficient for the face-on rich compared to edge-on interface, whereas charge recombination was suppressed in the latter.

Besides a high PCE, stability is also an important factor for the commercialization of OSCs. Chang *et al.* systematically compared the PCE and stability of the conventional BHJ and sequentially-processed (LBL) OSCs using a PTB7-Th/PC$_{71}$BM system, in terms of film morphology, molecular orientation, domain size and purity, vertical phase separation and charge transport. They observed that LBL OSCs without any additives exhibited a slightly higher PCE of 8.6% and excellent stability compared to that of the BHJ counterpart processed with 1.8-diiodooctane (DIO) as an additive (8.5%).[99] The LBL OSCs retained a PCE of 8.5% after heating at 130 °C for 120 min, while the BHJ devices reduced to 3.8%.

To improve the nanoscale morphology of BHJ OSCs some additional post-deposition treatments, such as thermal annealing and solvent vapor annealing are applied to the active layers. However, the optimal morphology of the blend is hard to achieve and control. These treatments can cause excessive or insufficient phase separation, which can reduce the efficiency of exciton dissociation or charge transport, leading to a reduction in the PCE of the OSCs. On the other hand, LBL OSCs prepared using sequential deposition avoids the problems of morphology control and phase separation. The polymer donor layer can crystallize without being disturbed by the top layer, with a more stable and reproducible morphology. This leads to higher PCEs for LBL OSCs compared to BHJ OSCs. Kim *et al.* observed that after the thermal annealing at 80 °C, the PCDTBT/PC$_{61}$BM-based LBL OSCs maintained 97.2% (from 5% to 4.89%) of its initial PCE for 10 days, while the efficiency of BHJ OSCs reduced to 37.5% (4% to 1.5%) of its initial value.[100] The grazing angle X-ray diffraction (GIXRD) and Flory–Huggins interaction parameter analysis indicated that the domain size of PCDTBT in the LBL active layer was greater than that of the BHJ counterpart and the ordered domains were still maintained after thermal annealing. The improved ordering of PCBTBT in the LBL film during thermal annealing prevents the mixing of PCDTBT and PC$_{61}$BM domains. However, the domain size of PCDTBT in BHJ was decreased due to the mixing of PCDTBT and PC$_{61}$BM domains during the thermal annealing, thus deteriorated the morphology of the BHJ layer.

Jang *et al.* prepared the LBL OSCs with PTB7/PC$_{71}$BM in which the PTB7 layer was prepared using a ternary solvent composed of CB, DIO and 1-chloronaphthaline (1-CN).[101] Addition of DIO and 1-CN solvent additives enhanced the PTB7 ordering in the thin film. GIXRD results demonstrated that the sequential deposition of the PTB7 and PC$_{71}$BM layers form the BHJ interlayer
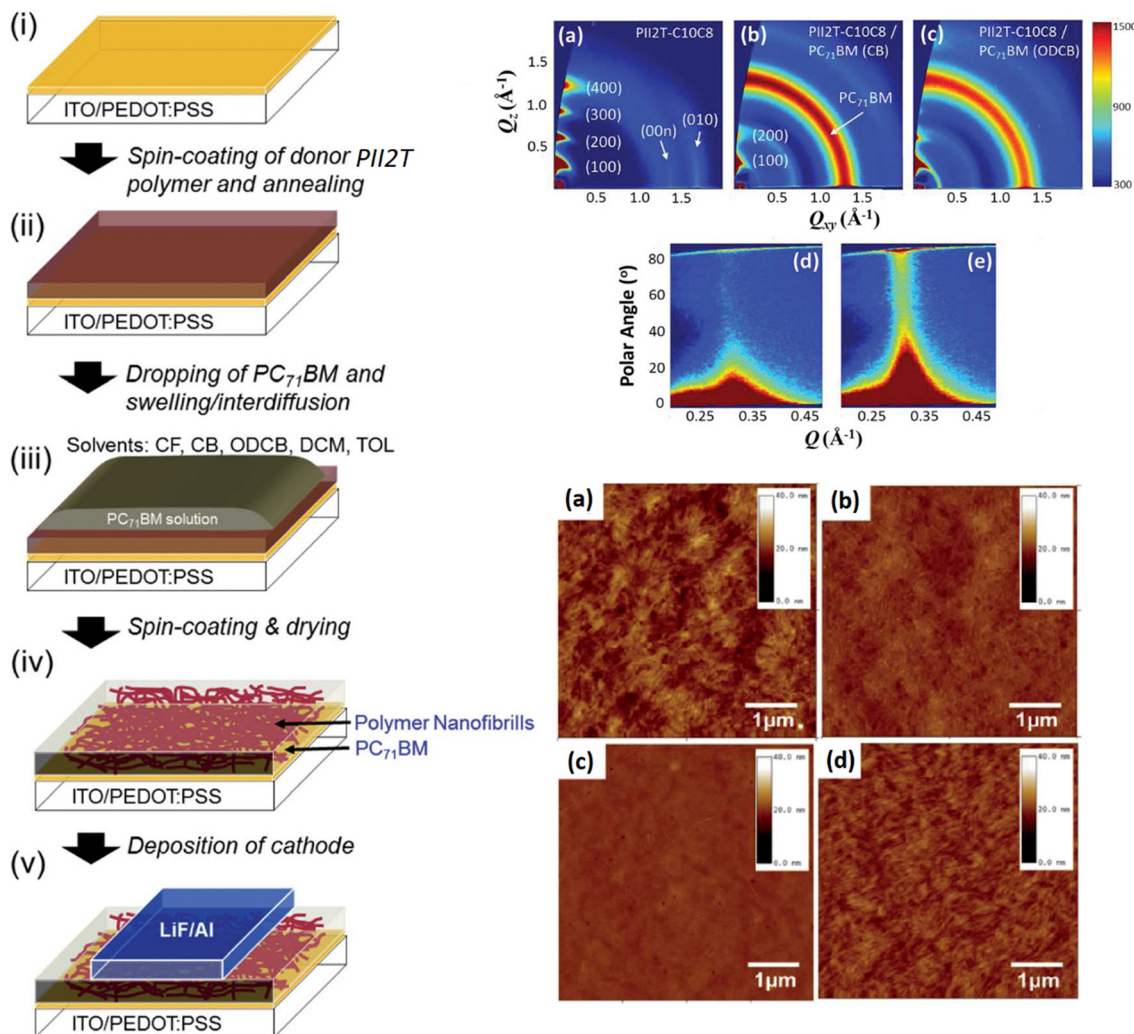
Fig. 8 Schematic representation of solution-processed sequential-processing of OSCs and the formation of a nanofibrillar structure induced by solvent swelling and interdiffusion of D/A. 2D GIXD patterns of (a) neat PII2T film and PII2T/PC$_{71}$BM SHJ films cast by PC$_{71}$BM derived from CB (b) and (d) and ODCB (c) and (e). Reprinted with permission from ref. 97. Copyright 2014, Royal Society of Chemistry.

with minor intermixing between PTB7 and PC$_{71}$BM domains compared with the conventional BHJ counterpart. OSCs employing an LBL-processed BHJ exhibited a PCE of 7.43% which was comparable to that of the BHJ counterpart. However, the LBL OSC maintained better stability compared to BHJ devices. Similar morphological stability improvement was also reported for LBL-processed OSCs using PCPDTBT/PC$_{71}$BM active layers which were dissolved in 1,2-dichloroethane (DCE) with low vapor pressure to reduce the swelling and minimize the intermixing of polymer with PC$_{71}$BM.[102]

The use of co-solvent for swelling of the bottom polymer layer during deposition is found to be an important part in forming the BHJ interlayer in LBL OSCs. Depositing the top PC$_{71}$BM layer from o-DCB formed an optimal morphology resulting in a PCE of 8.7% without any post-treatment which was higher than that of the BHJ device as well as the device processed from chloroform (CF), CB, and o-XY.[103] The swelling of the polymer (PffBT-3) layer by o-DCB improved the interfacial

BHJ layer formation and thus charge transport in the device. The results suggest that the solvent selection is very critical during LBL deposition to form gradient distribution of the phase in the vertical direction.

3.2. LBL-processed binary OSCs with fullerene-free acceptors

In fullerene-based OSCs, the poor absorption of fullerene derivatives in the visible region limits the PCE of the OSCs. On the other hand, A–D–A and A–DA'D–A-type fullerene-free acceptors (FFA) have strong absorption in the visible to near-infrared (NIR) region and have the advantage of tunable energy levels, which is beneficial for commercial applications.[3,5,48,51,104–109] The structures of fullerene-free acceptors (FFAs) are shown in Fig. 9 and 10. The first A–D–A-type acceptor reported was ITIC showing a PCE of about 6.8% in BHJ OSC.[30] But it was the A–DA'D–A-type Y6 acceptor whose development significantly boosted the PCE to over 15%.[31] Since then, significant advances have been made in the design and development of these materials leading to high PCEs
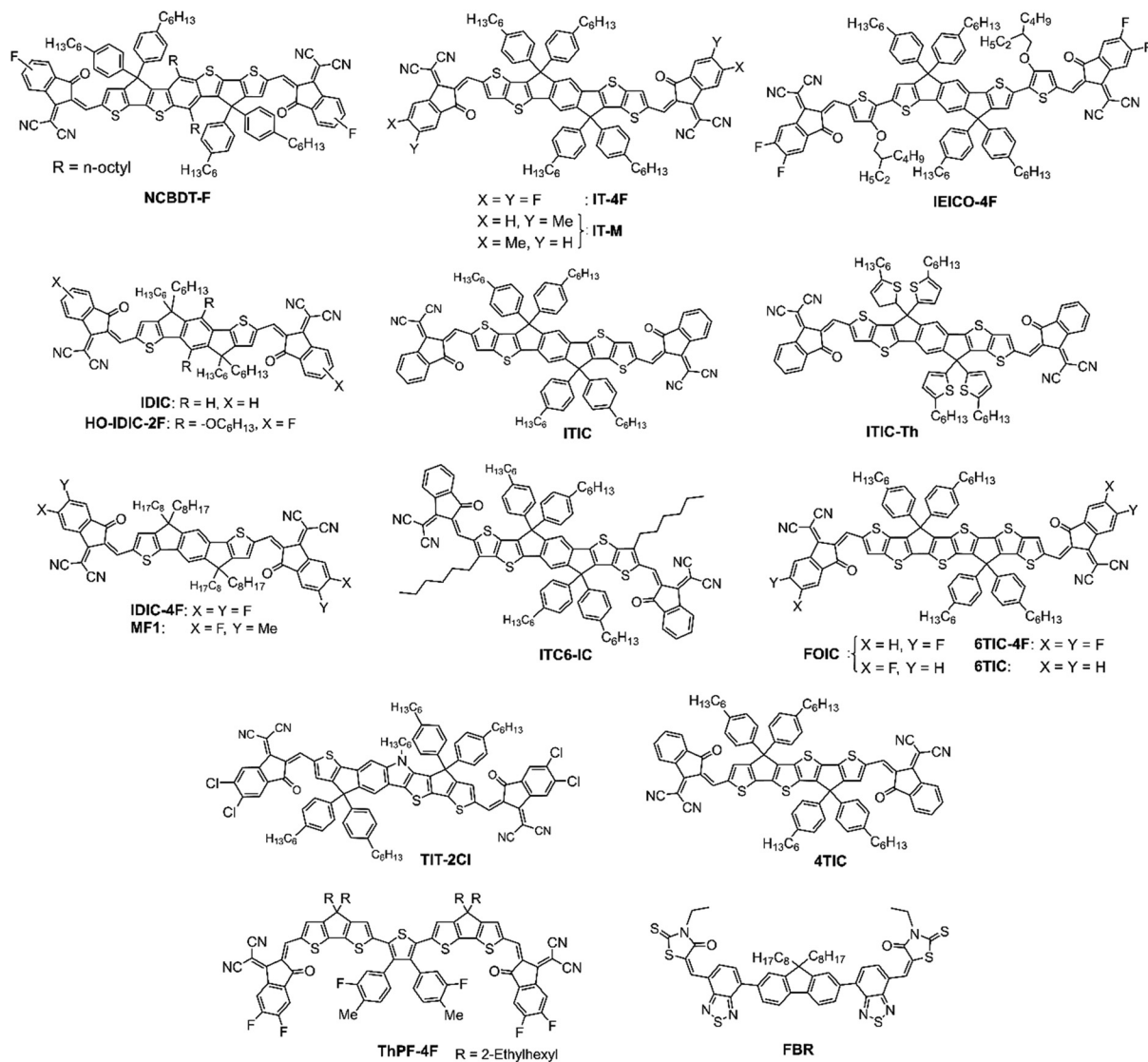
Fig. 9 Chemical structure of A–D–A-type fullerene-free acceptors.

above 19% achieved for BHJ devices prepared using binary or ternary blends. However, the control of morphology has been found to be very critical and more optimizations are required to achieve the best performance. In this respect, LBL processing was found to be a viable approach for performance enhancement in which the D and A layers are deposited sequentially.[64,68]

3.2.1. A–D–A-type fullerene-free acceptors. Friend's group prepared PBDB-T/NCBDT-F-based LBL OSCs by dissolving PBDB-T in CF and NCBDT-F in DCM and achieved a PCE of 10.04% with a V_{OC} of 0.82 V and J_{SC} of 19.45 mA cm^{-2}, respectively (Table 2).[70] They observed that the use of tetrahydrofurane (THF) instead of DCM completely washed away the underneath PBDB-T layer. Thus, the choice of solvent for the upper layer is very crucial which solubilizes the top materials but still protects the bottom layer. The charge generation efficiency in LBL OSCs is still higher despite having a small driving force of around 30 meV for exciton dissociation in LBL OSCs compared to BHJ OSCs.

A new polymer donor PBDB-TFS was synthesized by Cui *et al.*, by replacing the 2-ethylhexyl side chain of PBDB-TF with an *n*-octyl chain. This modification reduced the solubility of the polymer to protect it from top layer deposition and improved its photovoltaic performance.[71] They used CB and THF as solvents to sequentially deposit the D (PBDB-TFS) and A (IT-4F) layers, forming LBL OSCs. However, the device achieved a low PCE of 8.11% with high exciton recombination and low dissociation rate, suggesting that the PBDB-TFS and IT-4F layers did not intermix well to form a BHJ structure. When the IT-4F was dissolved in a mixture of *o*-DCB and THF, the *o*-DCB can solubilize the PBDB-TFS layer at higher temperature to attain an ideal morphology forming a p–i–n structure. The co-solvent *o*-DCB helped to infuse the IT-4F into the underneath polymer layer to form appropriate vertical phase distribution. Employing the conventional device structure ITO/PEDOT:PSS/PBDB-TFS/IT-4F/PFN-Br/Al, and optimizing the ratio of *o*-DCB:THF, a high PCE of 13.0% could be attained that was higher than that of the
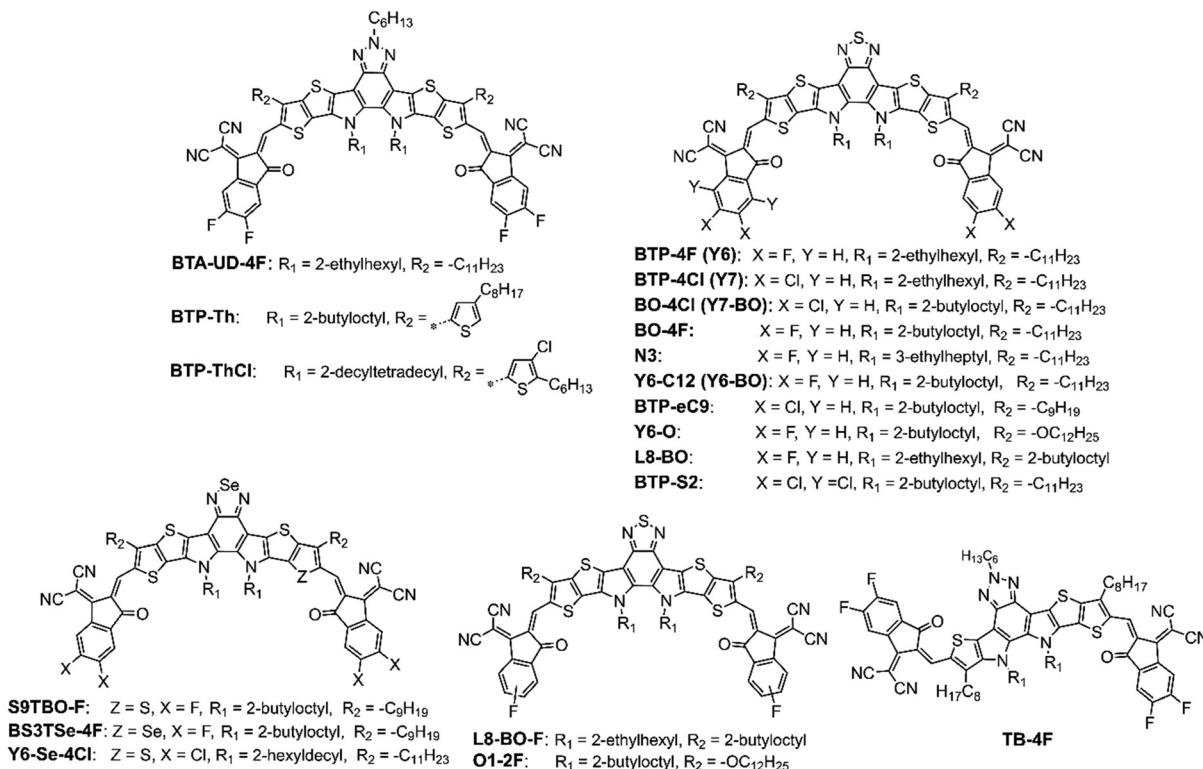
BTA-UD-4F: R_1 = 2-ethylhexyl, R_2 = $-C_{11}H_{23}$

BTP-Th: R_1 = 2-butyloctyl, R_2 =

BTP-ThCl: R_1 = 2-decyltetradecyl, R_2 =

BTP-4F (Y6): X = F, Y = H, R_1 = 2-ethylhexyl, R_2 = $-C_{11}H_{23}$
BTP-4Cl (Y7): X = Cl, Y = H, R_1 = 2-ethylhexyl, R_2 = $-C_{11}H_{23}$
BO-4Cl (Y7-BO): X = Cl, Y = H, R_1 = 2-butyloctyl, R_2 = $-C_{11}H_{23}$
BO-4F: X = F, Y = H, R_1 = 2-butyloctyl, R_2 = $-C_{11}H_{23}$
N3: X = F, Y = H, R_1 = 3-ethylheptyl, R_2 = $-C_{11}H_{23}$
Y6-C12 (Y6-BO): X = F, Y = H, R_1 = 2-butyloctyl, R_2 = $-C_{11}H_{23}$
BTP-eC9: X = Cl, Y = H, R_1 = 2-butyloctyl, R_2 = $-C_9H_{19}$
Y6-O: X = F, Y = H, R_1 = 2-butyloctyl, R_2 = $-OC_{12}H_{25}$
L8-BO: X = F, Y = H, R_1 = 2-ethylhexyl, R_2 = 2-butyloctyl
BTP-S2: X = Cl, Y =Cl, R_1 = 2-butyloctyl, R_2 = $-C_{11}H_{23}$

S9TBO-F: Z = S, X = F, R_1 = 2-butyloctyl, R_2 = $-C_9H_{19}$
BS3TSe-4F: Z = Se, X = F, R_1 = 2-butyloctyl, R_2 = $-C_9H_{19}$
Y6-Se-4Cl: Z = S, X = Cl, R_1 = 2-hexyldecyl, R_2 = $-C_{11}H_{23}$

L8-BO-F: R_1 = 2-ethylhexyl, R_2 = 2-butyloctyl
O1-2F: R_1 = 2-butyloctyl, R_2 = $-OC_{12}H_{25}$

TB-4F

Fig. 10 Chemical structure of A–DA′D–A-type fullerene-free acceptors.

Table 2 Solar cell data for the BHJ and LBL-processed OSCs with A–D–A-type fullerene-free acceptors

Active layer	Processing method	V_{OC} [V]	J_{SC} [mA cm^{-2}]	FF	PCE [%]	Ref.
PBDB-T/NCBDT	LBL	0.82	19.45	0.62	10.04	70
PBDB-T/NCBDT	BHJ	0.84	18.64	0.64	10.19	
PBDB-TFS/IT-4F	LBL	0.90	20.30	0.71	13.00	71
PBDB-TFS:IT-4F	BHJ	0.87	19.90	0.68	11.80	
PBDB-T/ITIC	LBL	0.86	15.30	0.50	7.00	110
PBDB-T:ITIC	BHJ	0.86	15.10	0.57	7.70	
PBDB-T-2F/IT4F	LBL	0.90	16.00	0.69	10.10	111
PBDB-T-2F/IDIC	LBL	0.95	14.90	0.69	10.00	111
J71/ITC6-IC	LBL	0.97	18.57	0.66	12.08	112
J71:ITC6-IC	BHJ	0.93	18.35	0.65	11.32	
PTQ10/IDIC	LBL	0.94	18.75	0.69	12.32	112
PTQ10:IDIC	BHJ	0.93	18.71	0.66	11.75	
PTQ10/HO-IDIC-2F	LBL	0.90	18.11	0.73	12.03	113
PTQ10/HO-IDIC-2F	BHJ	0.91	18.95	0.70	12.20	
PTFB-O/ITIC-Th	LBL	0.91	17.50	0.74	11.80	114
PTFB-O:ITIC-Th	BHJ	0.92	14.90	0.75	10.40	
PM6/IT-4F	LBL	0.86	20.98	0.75	13.70	115
PM6/IT-4F	BHJ	0.86	20.34	0.74	13.11	
FTAZ/IT-M	LBL	0.95	18.30	0.70	12.50	116
FTAZ/IT-M	BHJ	0.96	17.80	0.68	12.00	
PBDB-T/ThPF-4F	LBL	0.81	22.20	0.65	11.83	117
PBDB-T/ThPF-4F	BHJ	0.82	21.27	0.63	11.10	
PBDB-T:PC$_{71}$BM/ ThPF-4F	LBL	0.80	24.18	0.61	11.97	
PM7/IT4Cl	LBL	0.88	20.06	0.70	12.38	118
PM7:IT4Cl	BHJ	0.80	20.52	0.74	12.17	
PBTz-TC/IT-4F	LBL	0.86	20.54	0.68	11.96	119
PBTz-TC:IT-4F	BHJ	0.86	20.56	0.66	11.69	
PBTz-TTC/IT-4F	LBL	0.84	20.91	0.72	12.81	
PBTz-TTC:IT-4F	BHJ	0.84	20.61	0.71	12.42	

BHJ counterpart (11.8%). Moreover, after the addition of 15% *o*-DCB into THF solvent, the inverted LBL OSCs (ITO/ZnO/PBDB-TFS1/IT-4F/MoO$_3$/Al) achieved a PCE of 11.2%. The results demonstrated that the approach of employing a partial orthogonal solvent could create an intermixed morphology with favorable vertical D/A distributions, which could be effective for both conventional and inverted OSCs.

Huang *et al.* used PBDB-T as the donor and ITIC as the acceptor to fabricate inverted LBL OSCs employing the device structure ITO/ZnO/PBDB-T/ITIC/MoO$_3$/Ag and achieved a PCE of 7%.[110] Lee *et al.* selected a highly crystalline PBDB-TF donor and IDIC or IT-4F as the acceptor to fabricate LBL OSCs and achieved a PCE of about 10% which was comparable to the corresponding BHJ OSCs, with the advantage of simplified nanostructure formation.[111] The absorption spectrum of the IDIC acceptor overlapped significantly with the emission spectrum of the PBDB-TF donor, forming an effective exciton harvesting bilayer heterojunction. The organic bilayer heterojunction achieved efficient exciton diffusion by enabling long range energy transfer from the polymer donor (PBDB-TF) to the acceptor (IDIC).

Since most of the efficient polymer donors, such as PBDB-T, PBDB-TF, PTB7-Th, and FFAs ITIC, IT-4F, or Y6-series have similar solubility in organic solvents, it is hard to obtain orthogonal solvents to sequentially cast the D and A layers. So, non-orthogonal solvents are sometimes preferred to dissolve the D and A materials, when the orthogonal solvents have a limited option. It is also obvious that the semi-orthogonal

solvents could represent a preferable choice for deposition. During spin-coating of the upper layer from non-orthogonal solvent the bottom layer gets dissolved/swells and increases the surface roughness, thus forming a BHJ interlayer by mutual dispersion of D/A to promote exciton dissociation. Therefore, the active layer morphology of LBL devices exhibited a superior vertical structure compared with the conventional BHJ devices, which enhanced the charge transport and collection efficiency. Using different photoactive layers, Sun *et al.* constructed LBL OSCs by sequential solution-processing without orthogonal solvents and co-solvents.[112] The resulting OSCs with PTQ10/IDIC and J71/ITC6-IC as D/A pairs processed from CF attained PCE of 12.32% and 12.08%, respectively, which were higher than those of the corresponding BHJ OSCs (11.75% and 11.32%, respectively). They concluded that the strong absorption, reduced energy loss, enhanced vertical phase segregation, and partially increased charge transport and collection efficiency contributed to the PCE enhancement. Moreover, with the J71/ITC6-IC and PTQ10/IDIC combinations the large-area LBL OSCs (1 cm^2) prepared by doctor-blade coating under ambient conditions achieved PCEs over 10%. Huang *et al.* reported a simple and effective method to fabricate LBL OSCs using PTQ10 as the donor and HO-IDIC-2F as the acceptor, which were dissolved in THF. By spin-coating the acceptor layer from a cold THF solution, they prevented the dissolution of the underlying donor layer and achieved an appropriate D/A interface. The device exhibited a PCE of 12.03% without any additives or post-treatment.[113]

Yan and co-workers proposed an effective approach for the deposition of polymers which can only be solubilized in organic solvents at high temperature.[114] The donor layer was processed from TMB at high temperature forming a robust film which was not affected by any other solvents at room temperature. This will make the top acceptor layer deposit from nonorthogonal solvent at room temperature forming a p–i–n structure. They achieved PCEs of 11.8%, 11.6% and 11.7% for the LBL-processed PTFB-O/ITIC-Th-based OSCs using THF, CF, and toluene as solvents of different boiling points to process the acceptor and the PCEs obtained were higher than the BHJ OSCs (10.4%).

The mixing of additive either with the donor layer or the acceptor layer was found to be very crucial for device performance improvement. Chen and co-workers fabricated PM6/IT-4F based OSCs using DIO as the solvent additive.[115] When DIO was treated with PM6, the device generated a PCE of 12.11%, while a higher PCE of 13.7% was achieved when DIO was treated with IT-4F. The device without any additive also generated a PCE of 12.13% suggesting that the DIO treated PM6 layer does not affect the polymer crystallinity and bulk morphology. Whereas, the treatment of the IT-4F layer with DIO enhanced the crystallinity and phase separation as studied by GIWAXS and AFM studies and was beneficial for charge transport and collection.

The solvent used to process the bottom layer is equally important as for the top layer to improve the device performance. Ye *et al.* improved the molecular ordering of FTAZ polymer by regulating the solvent used for spin-coating and attained the best PCE of 12.5% based on FTAZ/IT-M bilayer OSCs.[116] The FTAZ donor was dissolved in *o*-XY, (*R*)-(+)limonene (LM), 2,6-dimethyl-anisole (DMA), TMB, or CB and the IT-M acceptor was dissolved in 2-methyltetrahydrofuran (2-MeTHF). The results demonstrated the highest domain spacing, when the donor film was prepared with LM, as confirmed from resonant soft X-ray scattering (RSoXS) experiment. The CB, DMA, and *o*-XY-processed device generated PCEs between 10.2% to 10.7%. The BHJ device gave a PCE of 11.9%. The improved PCE for the LM-processed device was due to suitable morphology with large phase separation (domain size of ∼35 nm).

Lin *et al.* observed an improved vertical gradient distribution of D and A in the LBL-processed PBDB-T/ThPF-4F OSCs to facilitate charge transport with reduced recombination losses compared to the BHJ counterpart.[117] The LBL-OSCs realized a PCE of 11.83% which was higher than the optimized BHJ counterpart (11.10%). When 10 wt% PC$_{71}$BM was added to the PBDB-T layer, the PCE was further enhanced to 11.97%.

Kang *et al.* demonstrated that the use of the LBL deposition method could suppress the nonradiative voltage losses in OSCs along with enhancement of electroluminescent quantum efficiency and thus increased the V_{OC} by 80 mV as compared to the BHJ device based on the PM7 donor and IT4Cl as the acceptor.[118] The suppression of aggregation in the film state was found to increase the energy level of intermolecular charge-transfer states and improve the interfacial charge transfer in LBL OSCs.

Deng *et al.* developed two polymer donors, PBTz-TC and PBTz-TTC, by introducing a BTz unit to enhance the film crystallinity and ester groups to improve the solubility and to lower the energy levels.[119] The planar PBTz-TTC has a strong film forming property in contrast to PBTz-TC. The orthogonal solvents were used to make the LBL OSCs, which affected the film properties of PBTz-TC and PBTz-TTC donors. PBTz-TC has a better balance between crystallinity and miscibility with an IT-4F acceptor compared with PBTz-TTC, leading to stronger D/A interaction at the interface. CF was used for the bottom donor layer and CB for the top acceptor layer deposition, which gave a PCE of 11.96% for the PBTz-TC/IT-4F device which is higher compared to the corresponding BHJ device. Furthermore, LBL OSCs processed with halogen-free solvent TMB using PBTz-TC/IT-4F achieved a PCE of 12.81% due to favorable morphology and efficient charge transport dynamics. The TMB-processed LBL device showed better stability maintaining about 82% of the initial PCE after 1200 h.

3.2.2. A–DA′D–A-type fullerene-free acceptors. Liu *et al.* achieved a PCE of 17.94% for the D18/Y6-based pseudo-bilayer device processed from CF as a single solvent (Table 3).[120] That means the bottom D18 layer can tolerate the CF processing of Y6. Meanwhile, the deposition of the D18 layer over the Y6 film led to a decrease in PCE to 7.8% due to the washing of the Y6 layer by CF.

Ning *et al.* developed two polymer donors by introducing linear or branched alkyl chains to the backbone.[121] The lower solubility of the linear alkyl chain containing polymer PNTB6-

Table 3   Solar cell data for the BHJ and LBL-processed OSCs with A−DA′D−A-type fullerene-free acceptors

Active layer	Processing method	V_{OC} [V]	J_{SC} [mA cm^{-2}]	FF	PCE [%]	Ref.
D18/Y6	LBL	0.86	27.24	0.76	17.94	120
D18:Y6	BHJ	0.86	26.75	0.75	17.36	
PNTB-Cl/N3	LBL	0.85	24.46	0.72	15.24	121
PNTB6-Cl/N3	LBL	0.85	26.58	0.77	17.59	121
PM6/N3	LBL	0.81	26.32	0.75	16.20	121
PBB-TSD/Y6	LBL	0.85	23.52	0.59	11.84	122
PBB-TSD:Y6	BHJ	0.87	21.19	0.58	10.77	
PM6/BO-4F	LBL	0.82	26.20	0.74	16.0	123
D18-Cl/Y6	LBL	0.86	26.86	0.76	17.73	124
D18/BS3TSe-4F	LBL	0.82	29.40	0.75	18.48	125
D18/BS3TSe-4F:Y6-O	LBL	0.84	29.41	0.76	19.03	
PM6/L8-BO	LBL	0.88	26.61	0.80	18.86	126
PM6:L8-BO	BHJ	0.88	26.25	0.78	18.18	
PM6/N3	LBL	0.86	26.75	0.79	18.10	127
PM6:N3	BHJ	0.85	26.93	0.76	17.10	
D18/L8-BO	LBL	0.91	26.86	0.77	19.05	128
D18:L8-BO	BHJ	0.91	26.31	0.75	18.14	
D18/L8-BO	LBL	0.93	26.43	0.74	18.02	129
D18:L8-BO	BHJ	0.92	24.54	0.73	16.43	
PT2/Y6	LBL	0.83	26.70	0.74	16.50	130
PT2:Y6	BHJ	0.83	26.30	0.68	15.00	
PM6/Y6-BO	LBL	0.84	26.20	0.77	17.20	131
PM6/Y6-BO	BHJ	0.84	25.80	0.75	16.40	
PM6/Y6	LBL	0.87	24.30	0.69	14.50	132
PM6:Y6	BHJ	0.85	25.00	0.72	15.40	
PM6/Y6	LBL	0.82	26.30	0.76	16.50	133
PM6:Y6	BHJ	0.85	25.30	0.73	15.80	
PNTB6-Cl/Y6-12	LBL	0.87	26.89	0.75	17.81	134
PNTB6-Cl:Y6-12	BHJ	0.87	26.45	0.74	17.33	
D18-Cl/Y6	LBL	0.86	27.17	0.76	18.16	135
D18-Cl:Y6	BHJ	0.87	27.02	0.73	17.38	
PNTB6-Cl/Y6	LBL	0.88	26.63	0.74	17.53	136
PNTB6-Cl:Y6	BHJ	0.85	23.78	0.73	14.81	
PM6/BTP-eC9	LBL	0.84	26.68	0.76	17.36	73
PM6:BTP-eC9	BHJ	0.85	26.72	0.73	16.80	
PM6:P-Cl/BTP-eC9:P-Cl[a]	LBL	0.85	27.81	0.80	19.10	73
PM6:P-Cl:BTP-eC9:P-Cl	BHJ	0.84	26.70	0.74	16.82	
D18/N3	LBL	0.83	27.79	0.75	17.52	137
D18:N3	BHJ	0.83	26.71	0.74	16.58	
PM6/Y6	LBL	0.85	27.74	0.77	18.16	138
PM6:FA-C12[b]/L8-BO	LBL	0.88	26.68	0.81	19.02	
D18/Y6	LBL	0.85	26.79	0.74	17.23	139
PM6/Y6	LBL	0.80	25.28	0.71	14.42	140
PM6/Y6-C12	LBL	0.80	23.80	0.56	10.60	141

[a] P-Cl was used as a polymer additive. [b] FA-C12 was used as a solid additive.

Cl in CF protected the polymer layer during the coating of the top acceptor layer, generating a smooth LBL film. While the film quality was not good for the CF soluble polymer PNTB-Cl. The PNTB6-Cl/N3 based LBL OSCs attained a PCE of 17.59%, which was superior to 15.24% obtained for PNTB-Cl/N3 based LBL OSCs and 16.2% for BHJ OSCs based on PM6:N3. These results demonstrated the significance of bottom layer solubility and its impact on the top layer penetration and phase separation in sequential casting.

Kang et al. compared the OSCs fabricated from LBL processing and conventional BHJ using a PBB-TSD donor and Y6 acceptor.[122] In comparison to BHJ the LBL films exhibited ordered molecular packing and appropriate D/A vertical phase separation, thus improving the exciton dissociation and reducing charge recombination. The resulting LBL OSC achieved a PCE of 11.84% that was higher than that of the BHJ device (10.77%).

Because of the limitation in materials solubility for BHJ deposition, Chen and co-workers used CB/THF as two orthogonal solvents to fabricate PM6/BO-4F-based LBL OSCs.[123] The PM6 polymer has good solubility in CB, while BO-4F is soluble in THF. The LBL device achieved a PCE of 15.6%. Further optimization of LBL films by using non-halogenated solvent o-XY for PM6 and THF for BO-4F deposition, resulted in an enhanced PCE of 16%. The BHJ device prepared using CF as the chlorinated solvent achieved a PCE of 16.5%. The results showed that the LBL method can be an effective strategy while using green processing solvent (non-halogenated) for layer deposition, while it is difficult to find a suitable green solvent for preparation of the BHJ layer.

Li et al. processed the D18-Cl donor layer from dual-solvent (CB + 5%THF) to balance the donor crystallization and morphology optimization. The spin coating of the Y6 layer from CF on top of the polymer donor allowed control of the morphology

of the donor layer and helped uniform penetration of Y6 into the D-layer.[124] The dual solvent processed LBL OSC with D18-Cl/Y6 attaining a PCE of 17.33% and 17.73%, when the polymer layer was coated from CF + CB and THF + CB mixtures, respectively. The devices were also reported to be stable after 2500 h retaining 90% of the PCE.

Gao *et al.* fabricated planar mixed heterojunction (PMHJ) OSCs by implementing the asymmetric selenium-containing acceptor, BS3TSe-4F with the D18 donor and compared the performance with the symmetric counterpart S9TBO-F.[125] The dielectric constant at the interface was enhanced by the more polarizable selenium, which also reduced exciton binding energy and helped exciton dissociation for free charge carrier generation. The Se-atom enhanced D–A dihedral angles and shortened the Se–O distance resulting in compact intra-molecular π–π stacking. The PMHJ OSCs using D18/BS3TSe-4F achieved a PCE of 18.48% and a high J_{SC} of 29.4 mA cm^{-2}. The D18/S9TBO-F device attained a PCE of 17.7%. The ternary PMHJ OSCs incorporating a medium bandgap Y6-O acceptor into D18/BS3TSe-4F improved the V_{OC} realizing a remarkable PCE of 19.03%. The PMHJ active layers showed smooth and even surfaces with low root-mean-square (RMS) roughness, as revealed by AFM measurements (0.86, 0.85 and 0.78 nm for D18/BS3TSe-4F and D18/S9TBO-F and the ternary layers) (Fig. 11a–c). This is suitable for the formation of ohmic contact with charge-transport layers. All active layers possess "face-on" orientation in the out-of-plane (OOP) direction (Fig. 11d–f), which facilitates the vertical transport of charge carriers.

He *et al.* compared the OSC performance of BHJ *versus* sequential deposition (LBL) using three D/A combinations *i.e.*, PM6/PC$_{71}$BM, PM6/L8-BO and PM6/IT-4F.[126] The LBL OSCs displayed higher performance compared to the BHJ devices by taking advantage of the appropriate vertical phase distribution due to the swelling process, and the LBL OSC based on PM6/L8-BO

achieved the best PCE of 18.86% (certified 18.44%). Also, the LBL OSCs showed improved charge transport and collection compared with the BHJ OSCs.

Zhao *et al.* observed faster charge extraction in the PM6/N3 active layer with effective suppression of bimolecular charge recombination and lower energetic disorder due to the superior crystallinity of the individual layers leading to improvement in the V_{OC} and FF.[127] The charge carrier lifetime measured from transient photovoltage measurements under open circuit conditions for the LBL OSCs is 2.62 μs, which is longer compared to the BHJ device (1.85 μs). Similarly, the transient photo-current measurement revealed a shorter charge extraction time for LBL OSCs (0.35 μs) compared with that of 0.46 μs for the BHJ device. The LBL-processed OSC achieved a PCE of 18.1% with enhanced stability compared with the conventional BHJ device with a PCE of 17.1%.

The performance of LBL-processed OSCs is significantly influenced by modification of the vertical component distribution as it impacts on the exciton dissociation, charge transport and recombination. The single-junction LBL OSCs based on D18/L8-BO exhibited a remarkable PCE of 19.05%, which was achieved by optimizing the film thickness of the active layer. This PCE was higher than that of the BHJ OSCs based on the same materials (18.14%), demonstrating the superiority of the LBL structure over the BHJ structure for OSCs.[128] One of the key factors that contribute to the high PCE of LBLOSCs is the appropriate distribution of vertical components. This distribution enhances the crystallinity of the active layer, facilitates the dissociation of excitons, reduces the energy loss, and ensures the balanced transport of charges.

Liu and co-workers fabricated LBL OSCs using a D18/L8-BO composition and found that by adjusting the temperature of the solution, they could manipulate the pre-aggregation state of the D18 donor material, which in turn affected the morphology
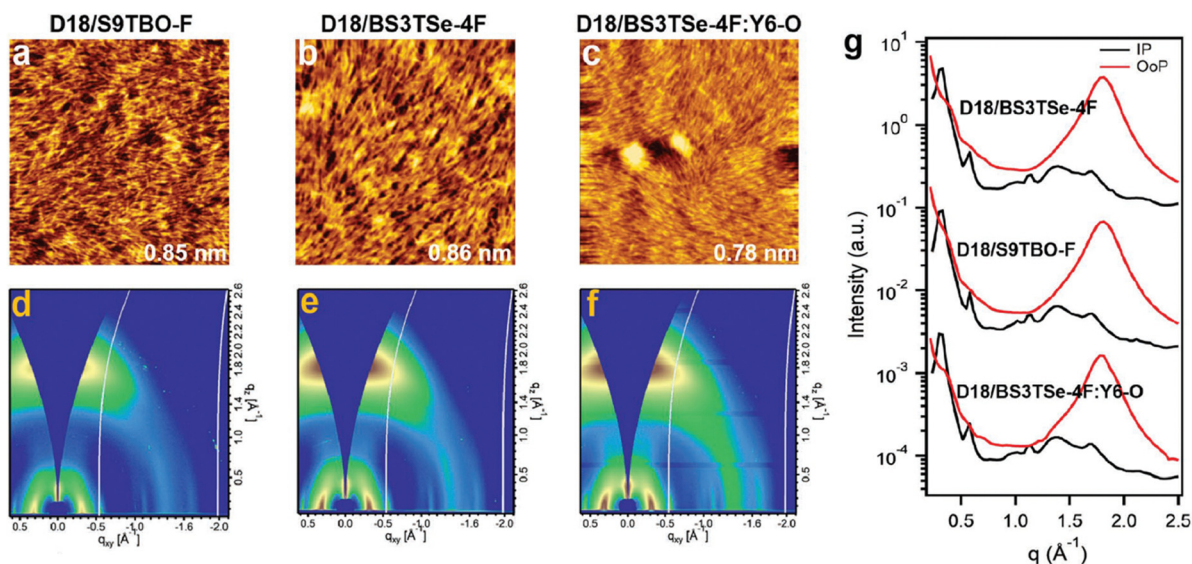

Fig. 11 (a)–(c) AFM height images (2 × 2 μm^2) and (d)–(f) 2D–GIWAXS patterns for the binary and ternary PMHJ films. (g) Corresponding GIWAXS line–cut profiles. Reprinted with permission from ref. 125. Copyright 2022, Wiley-VCH.

and performance of the OSCs.[129] The D18 layer can effectively regulate the film formation of the L8-BO upper layer resulting in a well-connected network for charge transport. Furthermore, vertical phase separation with a p–i–n-type D/D:A/A structure was achieved, which can enhance the light absorption and reduce the recombination losses in the device. By combining thermal annealing and solvent vapor annealing treatments, the optimized LBL OSC resulted in a PCE of 18.02%, which is higher than that for the BHJ counterpart (16.43%).

Solvent additive treatment is also an efficient approach to improve the OSC performance. An efficient p–i–n structure formation was achieved by Sun and co-workers, who adopted CB to process PT2 donor polymer and CF for the Y6 acceptor layer on top.[130] The addition of DIO during Y6 deposition was found to be very critical in performance improvement. The bottom polymer layer formed a self-assembled fibril network morphology. Then the Y6 diffused into the underneath polymer fibrils forming an optimal BHJ interlayer, which gave a PCE of 16.5% after DIO additive and thermal annealing treatment and is much higher than the BHJ OSCs (15.0%). The PT2/Y6 layer formed a stable morphology that is insensitive to batch variation of the polymer. Fu et al. constructed LBL OSCs using PM6/Y6-C12, (Y6-C12 also known as Y6-BO) where the 1-CN was introduced as the solvent additive to the acceptor Y6-C12 solution and achieved an excellent PCE of 17.2%, outperforming the BHJ counterpart (16.4%).[131] The high boiling solvent additive enhanced the film drying time of the molecule and assisted in the crystallization of the acceptor molecule. With the help of time-of-flight ion mass spectroscopy analysis, they observed that the Y6-C12 is present close to the hole transport layer. The studies indicated that Y6-C12 completely enters the PM6 layer, forming a channel that is beneficial for vertical charge transport. The method was also found to be compatible with other acceptors like Y6, IT-4F, IDIC-4F, and 6TIC-4F showing the significance of the LBL device compared with their BHJ counterpart.

Laquai's group constructed LBL OSCs by employing PM6/Y6 combination.[132] The bottom PM6 donor layer was coated from CB solution, while the top Y6 acceptor layer was deposited from low boiling CF solution containing 1-CN as a solvent additive. The optimized LBL OSCs with 0.5 vol% 1-CN attained a PCE of 14.5%, which is comparable to the BHJ counterparts.

Li et al. studied the control of vertical composition distribution in LBL-processed PM6/Y6 active layers using DIO as the solvent additive.[133] The addition of solvent additive enhances the inter-diffusion and optimizes the morphology of the quasi-planar heterojunction. The combination of vertical distribution of the active layer and improved crystallinity caused by 0.5% DIO aids in the exciton dissociation, charge transportation, and thus limiting the charge recombination losses. The slow drying of the Y6 layer allowed the improvement in molecular packing and diffusion of the Y6 molecules into the donor layer forming a BHJ with vertical phase distribution. The optimized PM6/Y6-based LBL OSCs yielded a PCE of 16.5% that was higher compared to the BHJ counterpart (15.8%). Moreover, the LBL processed PM6/Y6:PC$_{71}$BM ternary OSCs demonstrated an

excellent PCE of 17% with high stability up to 1500 h when stored under a N$_2$ atmosphere.

Ma et al. prepared LBL OSCs based on the PNTB6-Cl/BTP-4F-12 D/A layer (BTP-4F-12 named as Y6-C12).[134] The optimized LBL donor layer was deposited using diphenyl ether (DPE) in CB, while the BTP-4F-12 layer was deposited from DIO in CF solution. The solvent additives helped to improve the molecular ordering of both D and A layers and facilitated the formation of an efficient BHJ matrix between the D and A. The resultant LBL OSCs attained a slightly improved PCE of 17.81%, which was higher than the BHJ counterpart (17.33%).

Li et al. adopted a spin-coating method using solvent additives to prepare LBL films with precise control over the active layer morphology in D18-Cl/Y6 combination.[135] When the D18-Cl layer was prepared using n-octane as an additive the device reached a PCE of 17.70%. Similarly, the treatment of the Y6 layer with 1-fluoronaphthalene (FN) as an additive resulted in a PCE of 17.39%, which was higher compared to the BHJ OSCs (16.66%). Morphological studies indicated that n-octane in the donor layer reduced the surface roughness, and FN in the Y6 layer promoted the acceptor crystallization to facilitate charge transport. Furthermore, the LBL OSCs prepared by additive treatment of both the D18-Cl/Y6 layers reached an excellent PCE of 18.16% with a high J_{SC} of 17.17 mA cm^{-2} and FF of 0.77 due to the appropriate vertical morphology, favorable for exciton dissociation and charge collection. This indicates that the dual additive treatment slightly increased the degree of aggregation and reduced the D18-Cl/Y6 miscibility.

Xu et al. prepared LBL OSCs by sequentially spin-coating PNTB6-Cl polymer donor from CB and Y6 acceptor from CF solutions using DPE and 1,2-difluorobenzene (DFB) as solvent additive for the D and A, respectively.[136] The resultant OSCs exhibited a PCE of 17.53% with a FF of 0.75, higher than the PCE achieved for LBL-OSCs (16.38%) without solvent additives. The exciton dissociation at PNTB6-Cl/Y6 interfaces was further supported by improved exciton utilization efficiency through energy transfer from PNTB6-Cl to Y6. Under similar conditions the performance of LBL OSCs was higher compared to the BHJ counterparts indicating the significance of LBL-processed OSCs for further applications.

Recently, Zhou et al. used conjugated polymers (P–H, P–S, P–F and P–Cl with different side chains) as additives to optimize the active layer morphology of PM6/BTP-eC9-based LBL OSCs.[73] The polymer additive improved the PM6 fibril formation and facilitated the BTP-eC9 D/A network to form vertical separation with a better interconnecting structure. The morphology was fine-tuned by optimization of the alkyl side chain in the additives. The optimized device with P–Cl as the additive in the PM6 layer resulted in an impressive PCE of 19.1% with a FF of 0.80 that is slightly higher than the device without additive (17.36%). However, the addition of additive to the BHJ device did not show any PCE improvement (16.82%).

Huang and co-workers deposited a nonaromatic antisolvent (alkane, ether, and alcohol) layer after deposition of the bottom layer.[137] The antisolvent layer protects the damage of the bottom layer while coating of the top layer. The D18/N3-based device with

n-octane as the protecting solvent generated the best PCE of 17.52%. The best solvent was found to have a low saturated vapor pressure and high spreading coefficient.

Chen *et al.* added fatty acid (FA) molecules with variable carbon chain lengths (FA-C9, FA-C12 and FA-C16) as solid additives to the PM6 polymer donor solutions.[138] The solid additive approach enables the D and A to mix more easily and improve the interlayer morphology. This approach improved the charge transport and collection efficiency of OSCs and lowered the E_{loss} at the interface. The best results were obtained with FA-C12 and two acceptors, Y6 and L8-BO, reaching PCEs of 18.16% and 19.02%, respectively. The FA-treated devices showed enhanced performance compared to the BHJ and the LBL devices without FA.

Ma and coworkers, evaluated the influence of processing solvents on the film morphology and device performance of D18/Y6-based LBL OSCs processed by blade coating under ambient conditions.[139] The device performance mostly relied on the choice of solvent to deposit the donor layer. When the D18 donor layer was processed from CF solution the device yielded an excellent PCE of 17.23%. The top Y6 layer coated either from CF or CB favored BHJ interlayer formation and improved the acceptor crystallinity to facilitate efficient exciton dissociation with reduced charge recombination.

Yang and coworkers used slot-die coating to fabricate LBL OSCs under ambient conditions using PM6 as the donor and Y6 as the acceptor with CB and CF solvents of different boiling points without any additive and attained a PCE of 14.42%.[140] The device achieved high efficiency due to optimal vertical phase separation and enhanced charge transport and extraction derived from good quality film formation.

Welch and co-workers sequentially deposited the hole transporting PEDOT:PSS, photoactive D (PM6) and A (BTP-4F-12, also known as Y6-C12), and electron transporting PFN-Br layers using slot-die coating with non-halogenated solvents under ambient conditions.[141] Both the photoactive layers were deposited from *o*-XY forming an intermixing BHJ layer at the interface resulting in a PCE of 10.6%. When the Y6-C12 layer was deposited from 2-MeTHF the PCE reduced to 7.2% due to the formation of a more bilayer like structure.

The development of efficient OSCs for the Internet of Things (IoT) has received considerable interest in recent years. However, most studies have focused on the performance of OSCs under artificial light sources, neglecting the influence of natural sunlight in indoor environments. The artificial light only accounts for <35% of the total power density when combined with outdoor irradiation during the daytime. Therefore, together with artificial light, it is essential to consider the effect of sunlight on the indoor applications. Xie *et al.* synthesized an asymmetric FFA TB-4F and combined it with the PM6 donor to prepare LBL OSCs.[142] The LBL OSC under AM1.5 conditions achieved a PCE of 15.24% which is about 5% improvement as opposed to the BHJ device. However, under a 1000-lux LED (3000k) light source the TB-4F/PM6 LBL device showed a PCE of 21.05%, which is significantly higher in comparison to the BHJ device (16.82%). The improved performance of the LBL OSCs compared to the BHJ device under artificial light was due to reduced trap-assisted recombination, which increased the J_{SC} and FF and decreased leakage current, resulting in a higher V_{OC} under low charge carrier density.

To summarize, the LBL OSCs exhibit lower PCEs by using a fullerene acceptor, because the spherical structure of fullerene derivatives causes excessive aggregation forming grain boundaries which disturb the D/A interfaces' stability. This prevents the acceptor layer from effectively penetrating the donor layer and impeding appropriate phase separation for charge transport. On the other hand, FFAs with variable molecular shapes can effectively influence the π–π stacking, molecular orientation, absorption, and exciton dissociation. Furthermore, the LBL method offers the advantages of separately optimizing the morphology of the D and A layers, which is beneficial to improve the efficiency and stability of OSCs. The LBL method also improves the morphology and charge transport properties of the OSCs, resulting in enhanced performance compared to its BHJ counterpart. Another key parameter in the LBL method is the processing solvent which is extremely important along with the choice of the D/A materials. Mostly, the use of non-orthogonal solvent strongly affects the film formation, where the bottom layer can be washed away during the deposition of the top layer leading to poor device performance. The choice of orthogonal solvent for the deposition of D/A layers in LBL processing is an effective approach. The difference in solubility of D and A materials in orthogonal solvent has a significant role in individual film formation and avoids the loss of the bottom layer during washing. Using orthogonal solvent the bottom layer only swells due to the solvent, enhancing the interfacial quality. The processing of the crystalline donors from hot solvent leads to stable film formation, which enables the subsequent deposition of the top acceptor layer from a non-orthogonal solvent under ambient conditions. The use of high boiling solvent additives often showed metastable morphology of the films leading to poor device stability, thus solid additives have been introduced to obtain stable film morphology.

3.3. LBL-processed ternary OSCs

OSCs prepared using a ternary approach utilizing one (or two) electron donor(s) and two (or one) electron acceptor(s) was found to be very effective for performance improvement. However, it is very difficult to control and optimize the ternary BHJ morphology prepared in a single step. The bulk morphology was better controlled by the LBL deposition method in which the D and A layers are deposited sequentially. The morphology of LBL deposition films can be better controlled through the diffusion process using solvent additive and thermal annealing. The diffusion process clearly depends on the choice of solvent for the deposition of the upper layer.[143]

Cho *et al.* fabricated a ternary OSC *via* sequential deposition of one polymer donor and $PC_{71}BM$ + ITIC dual acceptor.[144] The fullerene derivative helped to form a bi-continuous charge transport pathway with the polymer and ITIC and improved the light absorption. The LBL processed ternary OSC achieved a PCE of 6.22% with enhanced stability compared to the BHJ devices (4.54%) (Table 4).

Table 4 Solar cell data for the BHJ and LBL-processed ternary OSCs

Active layer	Processing method	V_{OC} [V]	J_{SC} [mA cm^{-2}]	FF	PCE [%]	Ref.
PDCBT/PC$_{71}$BM:ITIC	LBL	0.87	10.12	0.71	6.22	144
PffBT4T-2OD/Y6:FBR	LBL	0.83	26.30	0.75	16.40	145
PffBT4T-2OD:Y6:FBR	BHJ	0.83	25.80	0.74	15.70	
PM6:N3:MF1	LBL	0.85	25.61	0.76	16.75	146
PM6:N3:MF1	BHJ	0.85	25.43	0.77	16.76	
PM6:IT-M/BTP-eC9	LBL	0.85	26.34	0.76	17.16	147
PM6:IT-M/BTP-eC9	BHJ	0.86	24.22	0.74	15.66	
PM6/BO-4Cl:BTP-S2	LBL	0.86	27.14	0.78	18.16	75
PM6/BO-4Cl:BTP-S2	BHJ	0.85	27.11	0.77	18.03	
PM6/Y6:TIT-2Cl	LBL	0.87	26.63	0.77	18.18	77
PM6/Y6:TIT-2Cl	BHJ	0.87	26.49	0.73	17.00	
D18-Cl:BTR-Cl/Y6	LBL	0.88	26.97	0.75	17.92	148
D18-Cl:BTR-Cl:Y6	BHJ	0.88	26.63	0.73	17.18	
PM6/Y7:BTA-UD-4F	LBL	0.85	27.40	0.75	17.55	149
PM6/Y7:BTA-UD-4F	BHJ	0.83	26.76	0.72	16.18	
PM6/BTP-eC9:L8BO-F	LBL	0.83	28.36	0.73	17.31	150
PM6/BTP-eC9:L8BO-F	BHJ	0.83	28.27	0.71	16.92	
PM6/Y6/PAEN	LBL	0.85	26.90	0.76	17.30	151
PM6:Y6:PAEN	BHJ	0.84	25.90	0.72	15.70	
PM6/N3:PC$_{71}$BM	LBL	0.84	26.49	0.78	17.42	152
PM6/N3:PC$_{71}$BM	BHJ	0.84	25.69	0.76	16.44	
PM6/Y6-O:PC$_{71}$BM	LBL	0.90	24.30	0.79	17.27	152
PM6/Y6-O:PC$_{71}$BM	BHJ	0.90	23.30	0.77	16.14	
PBB-TSD/PM6:Y6	LBL	0.85	26.83	0.76	17.71	154
PBB-TSD:PM6:Y6	BHJ	0.85	26.62	0.76	17.40	
Y6 (DSL)/D18-Cl/Y6	LBL	0.87	27.52	0.75	18.15	155
Y6 (DSL):D18-Cl:Y6	BHJ	0.86	25.35	0.72	15.81	
PM6/BO-4Cl:L8-BO	LBL	0.84	27.14	0.78	17.89	156
D18-Cl/BTP-eC9:BTR-Cl	LBL	0.86	27.31	0.78	18.21	157
PM6/BTR-Cl:Y7-BO	LBL	0.85	26.71	0.76	17.15	157
ZnP-TSEH/4TIC:6TIC	LBL	0.84	26.33	0.77	17.18	158
ZnP-TSEH:4TIC:6TIC	BHJ	0.81	25.95	0.75	15.88	
D18/3-BTP-ThCl:BTP-Th (2-CN)[a]	LBL	0.86	28.16	0.79	19.15	159
D18/3-BTP-ThCl:BTP-Th (DBB)[a]	LBL	0.86	27.98	0.78	18.73	159

[a] 2-CN and DBB were used as solid additives.

Using one polymer donor PffBT4T-2OD and two different FFAs (Y6 and FBR), Ren *et al.* created a series of ternary OSCs with the LBL deposition method. The maximum PCE achieved was 16.4%, which was higher than the 15.7% of the corresponding BHJ device with the same acceptor ratios.[145] For the LBL device the donor polymer was first deposited, then the acceptor's mixture with varying weight ratios was spin-coated on the top. The high efficiency for the LBL device was due to the controlled morphology forming a bicontinuous interpenetrating network of D and A for efficient charge transport and collection.

Xu *et al.* prepared LBL and BHJ-processed ternary OSCs employing a PM6 donor and two FFAs N3 and MF1.[146] Both LBL and BHJ ternary OSCs attained similar PCEs of 16.75% and 16.76%, respectively, which is ∼5% PCE improvement compared with the PM6:N3-based binary LBL or BHJ OSCs. The results demonstrated that the LBL approach is very effective in controlling the thickness of each layer while still maintaining a high device performance.

Li *et al.* constructed ternary OSCs using the PM6:IT-M/BTP-eC9 active layer processed from TMB by LBL blade-coating without any additives and post treatment.[147] The mixing of 20 wt% of IT-M to the PM6 donor protects the PM6 crystallization from the upper acceptor BTP-eC9, forming a dense nanofibril morphology, and resides within PM6 and BTP-eC9 to

form a cascade energy level alignment for efficient charge transfer leading to lowered recombination and improved V_{OC}. The LBL blade-coated OSCs attained a PCE of 17.16%. Zhan *et al.* reported PCEs of 18.16% for the ternary OSCs (PM6 donor and BO-4Cl:BTP-S2 FFAs) (BO-4Cl also named as Y7-BO) based on LBL processing in which 25 wt% of BTP-S2 was added in the acceptor mixture.[75]

In PM6:Y6-based BHJ OSCs over aggregation of the Y6 acceptor mainly restricts the device performance improvement. To suppress the aggregation of Y6, Chen *et al.* developed an unsymmetrical chlorinated FFA TIT-2Cl based on thieno-[3,2-*b*]indole and introduced it into the PM6:Y6 active layer. The insertion of Cl atom enhances the intramolecular charge transfer effect due to the higher dipole moment of the C–Cl bond. Furthermore the empty 3d orbital of Cl can act as a strong electron acceptor compared to the F atom. The PCE was enhanced from 15.78% to 17% through the use of TIT-2Cl as the third component due to improved light absorption, lowering of the energy level and charge transport.[77] The LBL-processed OSC prepared by spin-coating formed vertical phase distribution and enhanced the charge transport leading to a higher PCE of 18.18% with enhanced stability. The LBL OSC was prepared by first spin-coating the PM6 donor layer followed by deposition of mixed acceptors Y6:TIT-2Cl.

Zhu *et al.* reported LBL OSCs based on a D18-Cl/Y6 system which exhibited a higher PCE of 17.16% than the D18-Cl:Y6 BHJ OSCs (16.54%) due to adequate vertical distribution and reduced bimolecular recombination.[148] When a small molecule BTR-Cl was introduced to the D18-Cl/Y6 layer the crystallinity of the ternary blend was improved and the device attained the best PCE of 17.92% with a FF of 0.75. Recently, Gokulnath *et al.* prepared a ternary OSC by LBL processing from *o*-XY using a PM6/Y7:BTA-UD-4F active layer and attained a PCE of 17.55% which was higher than the BHJ-based ternary OSCs (16.18%).[149] Moreover, an impressive PCE exceeding 15% with an active layer thickness >300 nm was achieved. Cai *et al.* fabricated 300 nm thick film ternary LBL OSCs using a PM6 donor and two acceptors BTP-eC9:L8-BO-F achieving a PCE of 17.31% that was higher than that for the BHJ counterpart (16.92%).[150]

Bao's group applied a sequential deposition approach using orthogonal solvents to synergistically integrate ternary compositions by manipulating the addition process of a heat-resistant poly(aryl ether) (PAEN) insulator as the third component (Fig. 12).[151] PAEN was added in three different strategies; (1) the mixture of Y6 + PAEN was deposited on top of the PM6 donor to get t-PPHJ, (2) sequential deposition of PM6, PAEN and Y6 to get m-PPHJ and (3) deposition of the Y6 layer on top of the PM6 + PAEN layer to get b-PPHJ. The binary PM6/Y6 device without PAEN gave a PCE of 16.2% which was superior to the binary (PM6:Y6) (15.6%) or ternary (PM6:Y6:PAEN) (15.7%) BHJ devices. When PAEN was mixed with Y6 in the t-PPHJ device the PCE remain unchanged (16.2%). Meanwhile, the b-PPHJ device with PAEN at the bottom layer enhanced the PCE to 17%. Surprising, the OSCs with m-PPHJ configuration containing an intermediate PAEN layer generated the highest PCE of 17.3%. The enhancement of photocurrent was also seen from ΔEQE. The higher J_{SC} and FF for the m-PPHJ device was ascribed to the longer charge carrier lifetime and lower bimolecular and trap-assisted recombination processes. The concept was further validated using other acceptors like ITIC, IT-4F, and BTP-eC9 and the m-PPHJ OSC with PM6/PAEN/BTP-eC9 gave the best PCE of about 17.4%. The PAEN additive was also found to enhance the photo/thermal stability of the devices.

Jiang *et al.* reported a high efficiency OSC with an LBL method that outperformed conventional ternary BHJ devices using a PM6 donor and N3 and $PC_{71}BM$ dual acceptors.[152] The LBL film was prepared by deposition of the PM6 donor over the PEDOT:PSS layer followed by deposition of the N3:$PC_{71}BM$ mixture with 0.5% 1-CN from CF solution. The active layer was thermally annealed at 90 °C to form a pseudo-bilayer structure. Benefitting from the higher crystallinity, the LBL film exhibited a longer exciton diffusion length as studied by time-resolved photoluminescence (TRPL) measurements.[12,153] The exciton diffusion length estimated for the N3-phase (17.07 nm) in the LBL device is high compared with the BHJ layer (7.53 nm). Thus, despite having a larger average domain size (38 nm for the LBL film related to 26.5 nm for the BHJ film), the longer exciton diffusion length in the LBL film promoted efficient exciton dissociation. The photoluminescence decay lifetimes measured at 680 and 840 nm were also longer for the LBL film compared to BHJ, indicating the longer exciton lifetime in PM6 and N3 domains. Furthermore, the transient photocurrent (TPC) measurement revealed a shorter carrier extraction time of 0.94 μs for the LBL OSC compared with 1.12 μs in the BHJ OSC. Consequently, the PCE of the LBL OSCs was enhanced to 17.42% compared with 16.44% achieved for the BHJ device due to the high J_{SC} and FF values. Moreover, another
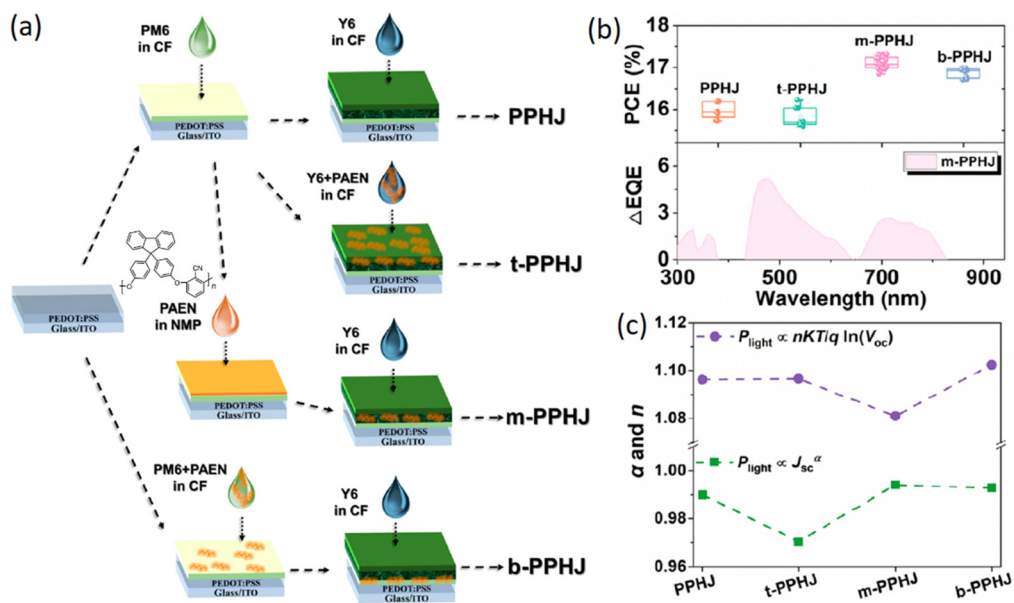

Fig. 12 (a) Layer–by–layer deposition strategies to influence the position of the poly(aryl ether) third component in PPHJ devices. (b) Box plots of PCEs development and EQE response for the PPHJ-type OSCs, where Δ_{EQE} = $EQE_{m\text{-}PPHJ}$ − EQE_{PPHJ}. (c) Dependences of V_{OC} and J_{SC} on P_{light}. Reprinted with permission from ref. 151. Copyright 2022, American Chemical Society.

LBL OSC consisting of PM6:Y6-O/PC$_{71}$BM attained a PCE of 17.27% suggesting the importance of the LBL technique.

In order to control the morphology without interfacial damage, Yan and coworkers used a ternary strategy with a PBB-TSD/PM6:Y6 composition.[154] The bottom polymer donor PBB-TSD was spin-coated from CF solution with DIO as the solvent additive and a blend of PM6:Y6 with 1-CN additive in CF was used as the top layer. The use of different solvent additives separately controlled the morphology of both the layers facilitating the formation of interfacial BHJ with vertical morphology and improved the charge collection efficiency. The optimized ternary BHJ OSCs processed with a sequential deposition method exhibited a PCE of 17.71% which is higher than that for the conventional BHJ ternary counterparts (17.40%).

Ma et al. fabricated D18-Cl/Y6 based LBL OSCs which yielded a PCE of 18.15% through the introduction of a dissociation strengthening layer (DSL) between the PEDOT:PSS and the D18-Cl donor compared to 17.62% for the device without the DSL layer.[155] The DSL layer helped to decrease the interfacial energy between the D and A, facilitating the molecular interdiffusion for efficient dissociation of charge carriers.

Tao and coworkers fabricated LBL OSCs using ternary components PM6/BO-4Cl:L8-BO exhibiting a PCE of 17.89%.[156] The two acceptors BO-4Cl and L8-BO formed an alloy model and enhanced the photon utilization efficiency and charge transport. The LBL processed binary OSC with PM6/BO-4Cl achieved a slightly lower PCE of 17.03% when processed from o-XY. Moreover, the device retained 89% of its original efficiency after 2000 h. The results demonstrated the viability of non-halogenated solvent for the development of high performance OSCs towards green energy technologies.

Li et al. proposed regulating the film morphology in LBL OSCs by diffusing a liquid crystalline BTR-Cl as the molecular donor into the fullerene-free host using non-halogenenated solvent o-XY.[157] The inclusion of BTR-Cl enhanced the crystallization leading to homogeneous D–A phase separation along the vertical direction, thus improving the charge transfer and lowering the voltage loss, thus achieving an impressive PCE of 18.21% for D18-Cl/BTP-eC9:BTR-Cl ternary OSCs. The device based on PM6/Y7-BO:BTR-Cl achieved a PCE of 17.15%.

Li and coworkers reported a high performance all-small molecule LBL OSC by using methoxy-substituted graphdiyne (GOMe) as solid additives.[158] The addition of GoMe helped to control the morphological growth and vertical component distribution, forming an optimal BHJ sandwich between the D (ZnP-TSEH) and A (4TIC:6TIC) enriched bottom and top layers. The addition of GoMe to the donor layer enhanced the surface roughness, thereby facilitating the diffusion of acceptor and formation of vertical phase distribution. In addition, the GoMe containing acceptor layer formed compact molecular packing with efficient pathways for exciton dissociation and charge transport. The best device reached a PCE of 17.18% with an FF of 0.77, compared to 15.88% for the BHJ device.

Recently, Jen and co-workers incorporated solid additives with different electrostatic potential (ESP) distributions and

steric hindrance into the active layer components in LBL-OSCs to examine how evaporation dynamics and selective interaction affected vertical component distribution.[159] A comparative study of different solid additives reveals that p-dibromobenzene (DBB) enhances the interaction with the donor, while 2-chloro-naphthalene (2-CN) favors interaction with the acceptor. Ternary OSCs employing D18/3-BTP-ThCl:BTP-Th (1:0.8:0.2) as the active layer with DBB and 2-CN as solid additives, attained PCEs of 18.73% and 19.15%, respectively.

In this study, the ternary OSCs prepared using LBL-strategies were found to show high efficiency. The use of non-halogenated solvent, sequence of addition, and solid additive processing were also found to be important for performance improvement. They helped to adjust the interfacial morphology and create the optimal BHJ structure. The LBL device achieved high efficiency because the morphology was controlled to form a network of interpenetrating D and A domains that enabled effective charge transport and collection.

3.4. LBL-processed multicomponent OSCs

Like the ternary blend, preparation of the quaternary blend could be another choice, which can broaden the absorption band for light absorption. However, the major problem in the processing of the quaternary blend is the control of miscibility of materials and optimization of blend morphology. In this respect, coating two BHJ layers over one another found to be practically more feasible. In this method two binary blends are coated sequentially without any need for morphology optimization. The layers can be of D1:A/D2:A, D:A1/D:A2, D1:D2/A1:A2, and D1:A1/D2:A2 configurations. One must take care of the stability of the bottom layer while processing the top layer by choosing appropriate solvent. The bottom layer materials should be stable during top layer deposition. The film formation for double-BHJ coating is quite different in contrast to the individual binary films. Ade and co-workers used a less soluble polymer donor PDPP3T and deposited the PDPP3T/PC$_{71}$BM layer on the ITO/ZnO substrate, and then deposited the FTAZ/PC$_{71}$BM layer at room temperature from the same solvent forming a pseudo-bilayer structure. The double-BHJ ternary device gave a PCE of 6.73% higher than the conventional ternary and binary devices (4.4–6.4%) (Table 5).[160] Huang et al. reported a PCE of 12.25% for PDPP3T:PC$_{71}$BM/PTB7-Th:PC$_{71}$BM-based OSCs in which [5,6]-open azafulleroid, a fullerene derivative was coated over the ZnO layer to promote electron transport from BHJ to the ZnO layer.[161] Similarly, Janssen's group achieved a PCE of 5.9% with PDCB-2T:PC$_{71}$BM/PDPP2T-TT:PC$_{71}$BM bilayer ternary OSCs prepared by spontaneous spreading on water.[162]

Wang et al. demonstrated the formation of controlled crystallization using a PBDB-T:IT-M/PBDB-T:FOIC double BHJ structure, which favors reduced recombination and better charge transport.[163] However, the binary PBDB-T:FOIC blend showed large phase separation, resulting in lower photocurrent. A double-BHJ OSC was prepared by sequential deposition of two binary blends with PM6 as the donor with Y6 and Y6-Se-4Cl as two acceptors.[164] The PM6:Y6 was deposited by printing

Table 5 Solar cell data for the BHJ and LBL-processed multicomponent OSCs

Active layer	Processing method	V_{OC} [V]	J_{SC} [mA cm^{-2}]	FF	PCE [%]	Ref.
PDPP3T:PC$_{71}$BM/FTAZ:PC$_{71}$BM	LBL	0.69	15.67	0.61	6.73	160
PDPP3T:FTAZ:PC$_{71}$BM	BHJ	0.63	12.01	0.65	5.09	
PDPP3T:PC$_{71}$BM/PTB7-Th:PC$_{71}$BM	LBL	0.77	23.75	0.67	12.25	161
PDCB-2T:PC$_{71}$BM/PDPP2T-TT:PC$_{71}$BM	LBL	0.68	14.9	0.58	5.90	162
PBDB-T:IT-M/PBDB-T:FOIC	LBL	0.75	24.66	0.63	11.91	163
PM6:Y6-Se-4Cl/PM6:Y6	LBL	0.84	26.3	0.73	16.40	164
PM6:PM7/Y6:O1-2F	LBL	0.86	26.97	0.78	18.23	165
PM6/Y6	LBL	0.84	26.52	0.75	17.00	165
D18-Cl:BTP-eC9/PM6:L8-BO	LBL	0.89	27.02	0.80	19.61	72
D18-Cl:PM6:L8-BO:BTP-eC9	BHJ	0.88	26.29	0.68	15.83	
PM6:Y6/PM6:Y6	LBL	0.84	26.63	0.79	17.73	166
PTQ10:Y6/PTQ10:Y6	LBL	0.85	26.70	0.78	17.81	166

onto the PM6:Y6-Se-4Cl film using polydimethylsiloxane stamps to avoid any damage to the bottom layer. The PM6:Y6-Se-4Cl/PM6:Y6 inverted OSC gave a PCE of 16.4% compared to 15.0% (PM6:Y6-Se-4Cl) and 15.4% (PM6:Y6) for the individual BHJ devices. The bilayer structure provides a favorable vertical gradient facilitating charge transport.

Li and coworkers used the combination of a quaternary concept with LBL deposition in which the active layer was prepared by deposition of a two acceptor blend (Y6:O1-2F) on top of the two donor (PM6:PM7) film.[165] The donor combination facilitated efficient charge transfer due to cascade energy level alignment, while the poor miscibility of the acceptor O1-2F with the donors favored vertical phase separation with the formation of a charge transport channel. The alloy acceptor Y6:O1-2F can optimize the vertical and horizontal morphology of the active layer for efficient charge separation and transport. Consequently, the PM6:PM7/Y6:01-2F system delivered a reduced non-radiative loss (0.231 eV) compared to a PM6/Y6 binary OSC, attaining a high PCE of 18.23%.

Xu et al. applied sequential processing and fabricated a pseudo-bilayer heterojunction (PBHJ) structure using D18-Cl:BTP-eC9/PM6:L8-BO pairs.[72] The bilayer was prepared by depositing the PM6:L8-BO mixture in CF over the D18-Cl:BTP-eC9 film prepared from hot CF, which cannot deliberately damage the underneath layer (Fig. 13). In contrast, deposition of the D18-Cl:BTP-eC9 layer over PM6:L8-BO film from hot CF could easily remove the bottom layer. The double-BHJ (multicomponent) OSCs displayed improved light absorption with balanced morphology compared to the conventional quaternary blend. Contrary to the devices with a quaternary blend, the double BHJ bilayer OSC showed lower non-radiative energy loss (ΔE_3), thus, achieving an exceptional PCE of 19.61% (the highest value to date) that is higher than the binary BHJ counterparts (18.25% for D18-Cl:BTP-eC9 and 18.69% for PM6:L8-BO) and the quaternary BHJ device (15.83%). Morphological issues could be the reason behind the low performance of the quaternary blend. The individually deposited optimized BHJ layers exhibited a higher molecular ordering than the quaternary blend. The improved crystallinity of the multijunction layers could facilitate the charge transport in OSCs. Li et al. used a PBHJ strategy to deposit two layers of the same D:A blends using a low donor concentration (4 mg mL^{-1} for donor). The PBHJ-based on

PM6:Y6 and PTQ10:Y6 exhibited high PCEs of 17.73% and 17.81%, respectively, because of the efficient exciton dissociation and balanced charge transport in the pseudo-bilayer.[166]

3.5. LBL-processed all-polymer OSCs

Phase separation at the nanoscale is a prerequisite to balance exciton dissociation and charge transport in BHJ OSCs.[52,167,168] This requires appropriate mixing of D:A in the blend solution and deposition of the film to form the desired crystallites at the nanoscale. The control of active layer morphology in all-polymer OSCs is even critical for its performance improvement. The unusual phase separation and oversize growth of crystallites is the major issue ensuing from the thermodynamically unfavorable mixing of both D and A polymers. Usually, the polymer chains are highly anisotropic and hinder appropriate molecular interactions and packing/orientation, affecting the charge generation and collection in the device.[169,170] Important issues that could be raised in all-polymer OSCs are their miscibility in orthogonal solvents to prevent dissolution by the top layer coating and ordering of the bottom layer. In this context, two-step LBL processing could be an efficient approach to precisely control the phase separation and packing. The structures of polymeric fullerene-free acceptors (FFAs) are shown in Fig. 14.

To avoid the solubility issues of the D and A polymers, Ma and co-workers used an LBL method in which the polymer donor PBDB-T in CF solution was deposited over a naphthalene-diimide-based D–A-type polymer acceptor N2200. The poor solubility of N2200 in CF facilitated the ordering of a PBDB-T layer forming a p–i–n structure. The LBL device gave a PCE of 9.52%, which is significantly higher than the BHJ OSC (6.58%) (Table 6).[171] The better efficiency was further supported by transient absorption studies which showed about 62% hole transfer efficiency for the LBL device compared to only 49% for the BHJ device.[172]

Zhong and coworkers used a perylene-based polymer acceptor FPDI-BT1 and demonstrated the formation of preferred bicontinuous interpenetrating BHJ configurations in all-polymer OSCs using PBDB-T/FPDI-BT1 prepared by sequential processing with the same solvents without any post treatments.[173] The morphology can be effectively tuned by the solvent used for processing of the top layer. The bottom layer was processed
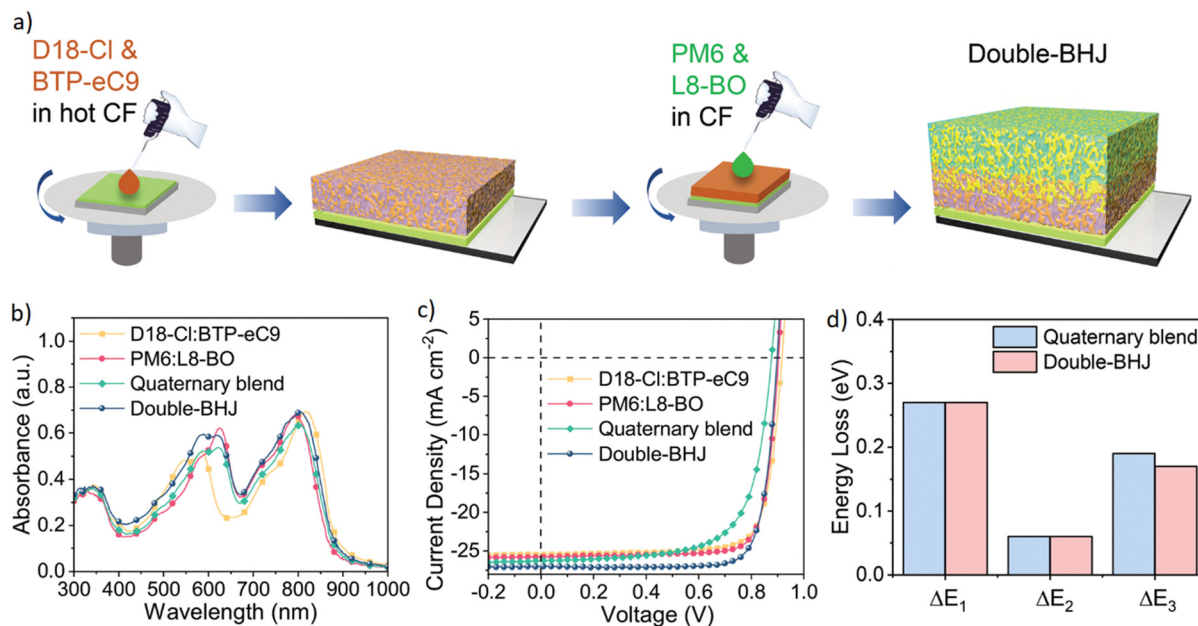
Fig. 13 (a) Schematic representation of the multicomponent OSCs prepared by sequential deposition. (b) Absorption spectra of the active layers. (c) Corresponding J–V curves. (d) Energy loss in the devices. Reprinted with permission from ref. 72. Copyright 2023, Wiley-VCH.
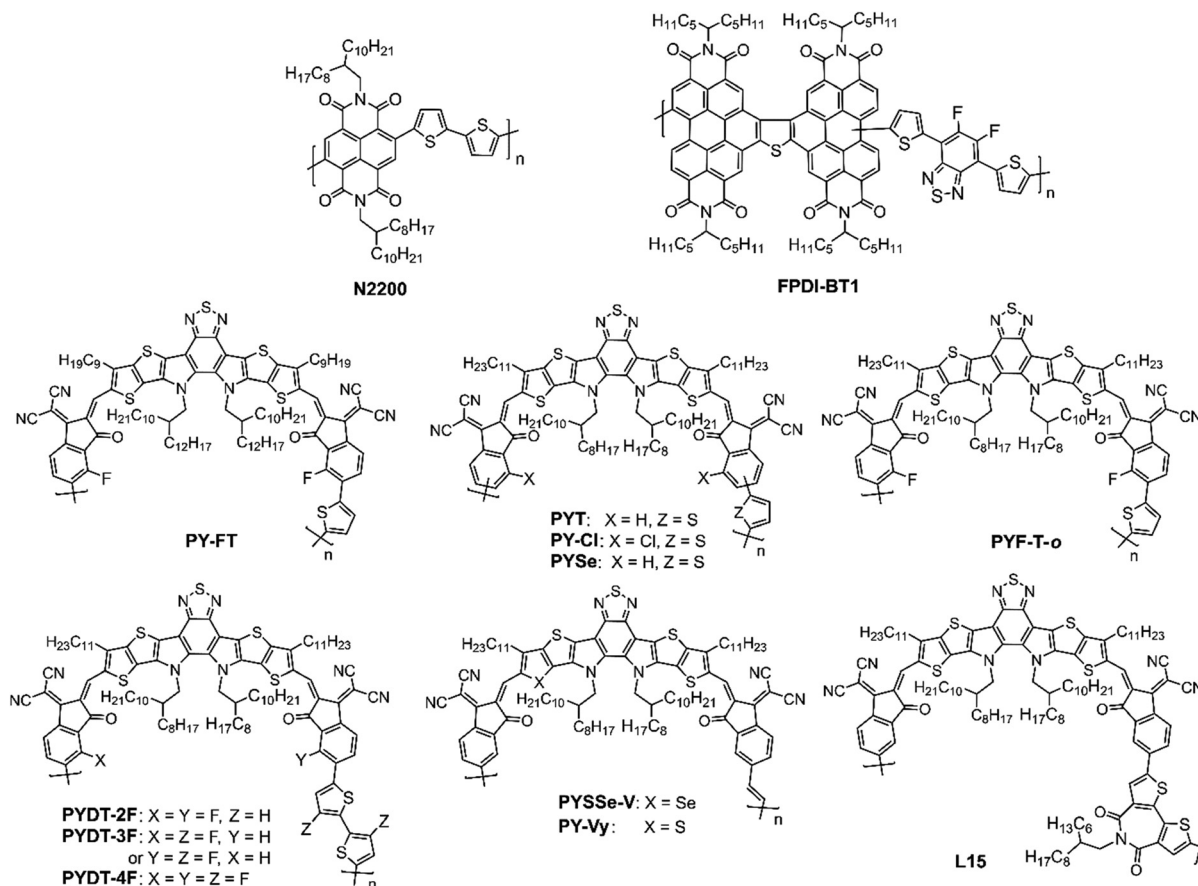

Fig. 14 Structure of ring-fused heteroacene-based polymer acceptors.

Table 6 Solar cell data for the BHJ and LBL-processed all-polymer OSCs

Active layer	Processing method	V_{OC} [V]	J_{SC} [mA cm^{-2}]	FF	PCE [%]	Ref.
PBDB-T/N2200	LBL	0.90	15.33	0.69	9.52	171
	BHJ	0.87	11.89	0.64	6.58	
PBDB-T/FPDI-BT1	LBL	0.96	11.63	0.61	7.15	173
PBDB-T:FPDI-BT1	BHJ	1.00	7.40	0.46	3.57	
D18/PY-FT	LBL	0.92	24.20	0.76	17.00	174
D18:PY-FT	BHJ	0.92	23.10	0.72	15.40	
PM6/PY-IT	LBL	0.95	22.61	0.73	15.81	175
PM6:PY-IT	BHJ	0.95	21.29	0.72	15.29	
PBDB-T/PYT	LBL	0.91	23.07	0.77	16.05	176
PBDB-T/PYT	LBL	0.89	23.03	0.73	15.17	177
PBDB-T:PYT	BHJ	0.88	22.64	0.70	14.06	
PBDB-T:PYT	LBL	0.89	22.95	0.74	15.10	177
PBDB-T/Y6	LBL	0.71	25.94	0.61	11.44	177
PBDB-T:Y6	BHJ	0.71	25.50	0.59	10.68	
PM6/PYDT-2F	LBL	0.93	24.11	0.72	16.25	178
PM6/PYDT-3F	LBL	0.92	24.49	0.77	17.41	
PM6/PYDT-4F	LBL	0.91	24.37	0.75	16.77	
PM6/PYSSe-V	LBL	0.90	25.20	0.75	17.03	179
PM6/PY-Cl	LBL	0.90	24.85	0.73	16.37	179
PM6/PYSSe-V:PY-Cl	LBL	0.91	25.88	0.77	18.14	179
PM6/PYF-T-o	LBL	0.90	25.16	0.69	15.82	180
PM6:PYF-T-o	BHJ	0.89	23.51	0.67	14.21	
PM6/PY-IT	LBL	0.93	22.54	0.70	14.86	180
PM6:PY-IT	BHJ	0.93	23.70	0.66	14.80	
PBQX-H-TF/PYSe	LBL	0.91	23.49	0.73	15.77	181
PBQX-H-TF:PYSe	BHJ	0.91	23.17	0.65	13.91	
PM6/L15	LBL	0.94	23.58	0.73	16.15	182
PM6/L15	BHJ	0.95	22.51	0.71	15.19	
PM6/PY-V-γ	LBL	0.90	24.50	0.76	17.00	183
PM6:PY-V-γ	BHJ	0.91	24.30	0.73	16.30	

from DCB. The use of CB for the top layer led to the formation of a bilayer structure with a PCE of 3.33%, which was improved to 7.15% with DCB as the top layer processing solvent due to the formation of an ideal morphology with a highly crystalline and ordered network of D/A polymers. The corresponding BHJ device gave a lower PCE of 3.57%.

Fu *et al.* adopted a top-down method to manipulate the morphology of all-polymer OSCs prepared *via* LBL deposition.[174] The top polymer acceptor was deposited from CF or toluene solution over the polymer D18 layer. The D18 polymer donor was partially soluble in CF but is insoluble in toluene, thus controlling the swelling of the bottom layer and formed an intermixed layer with polymer acceptor PY-FT. Thus, optimization of the top layer deposition with toluene formed a favorable vertical distribution at the nanoscale realizing a high PCE of 17% with a FF of 0.76. When the top layer was deposited from CF the device generated a PCE of 16.2% showing the influence of bottom layer orientation and top layer ordering on the performance improvement due to efficient charge generation and transport. The BHJ device processed from CF resulted in a slightly lower PCE of 15.4%. The LBL devices showed high stability retaining > 90% of their initial PCEs when kept at 65 °C for 1300 h.

Xu *et al.* constructed all-polymer LBL OSCs with PM6 as the donor and low bandgap polymer PYT as the acceptor and compared them with BHJ active layers.[175] The optimized OSCs based on LBL and BHJ active layers using 1 vol% 1-CN in PYT solution, attained PCEs of 15.81% and 15.29%, respectively. Zhang *et al.* demonstrated the application of 1-CN as the

solvent additive for the top polymer acceptor (PYT) deposition followed by thermal annealing to improve the lamellar ordering of the bottom PBDB-T polymer and vertical phase distribution in the active layer.[176] The LBL processed all-polymer PBDB-T/PYT OSCs attained a PCE of 16.05% with a FF of 0.77 due to favorable morphology, efficient exciton dissociation and suppression of charge recombination losses. Wu *et al.* fabricated all-polymer OSCs based on LBL processed PBDB-T/PYT by both spin-coating and blade coating and achieved PCEs of 15.17% and 15.10%, respectively, which were higher than the BHJ counterparts (~14.1%).[177] The active layer morphology was regulated by varying the additive dosages. The solvent additive was optimized with both polymer donor and acceptor and the best PCE and high FF was achieved by mixing 2.5 vol% of 1-CN with only a PYT acceptor during the deposition (Fig. 15). At the same time LBL processed PBDB-T/Y6 based OSCs achieved a PCE of 11.44% by mixing 0.2% 1-CN with PBDB-T donor and 0.5% with Y6 acceptor for optimizing the D/A mixing.

Recently, three narrow bandgap polymer acceptors named PYDT-2F, PYDT-3F and PYDT-4F were developed and all-polymer OSCs using PM6 as the donor polymer, processed *via* the LBL method, achieved a PCE of 17.41% with a FF of 0.77 for PM6/PYDT-3F which was higher than that for PM6/PYDT-2F (16.25%) and PM6/PYDT-4F (16.77%).[178] The polymer miscibility was enhanced by increasing the F contents in the acceptor which facilitated the formation of fibrillar nanostructure. The PM6 donor layer was deposited from CB and the upper acceptor was spin-coated using low boiling solvent CF + 2 vol% 1-CN,
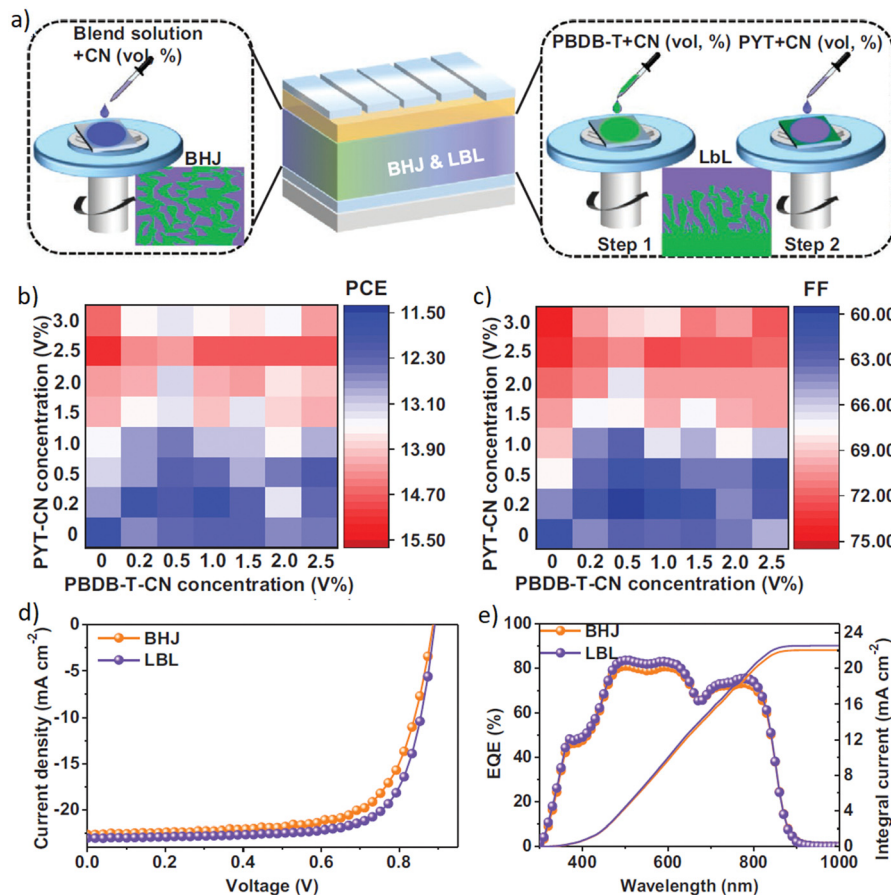
Fig. 15 (a) Representation of BHJ and LBL OSC processing. (b) PCE and (c) FF of the PBDB-T/PYT LbL all-polymer OSCs as a function of 1-CN content for each layer. (d) J–V characteristics and (e) the equivalent EQE spectra for the optimized devices. Reprinted with permission from ref. 177. Copyright 2021, Wiley-VCH.

which is very advantageous to form vertical phase separation. This strategy was found to be very effective for morphology optimization in all-polymer OSCs.

Min and coworkers synthesized two polymerized Y6 acceptors, named PYSSe-V and PY-Cl and introduced them as the top layers to fabricate the LBL binary all-polymer OSCs with PM6 as the bottom donor layer.[179] Replacing sulfur with selenium atom in PYSSe-V resulted in a greater ground state quinoidal character due to its loose π-electron delocalization, leading to lowering of the bandgap, thus helping to improve the photocurrent (J_{SC}). Aided by the broad absorption coverage and controlled vertical phase separation of the LBL processed active layers, PCEs of 17.03% and 16.37% were achieved for PM6/PYSSe-V and PM6/PYCl OSCs, respectively. The LBL ternary OSC with PYSse-V : Py-Cl acceptors (1 : 1) as the top layer showed a balanced vertical phase dissemination with a rich donor bottom layer. This impedes the charge recombination and enhanced the charge transport and collection, resulting in a PCE of 18.14% for all-PSCs.

Zhao *et al.* fabricated sequential LBL-deposited all-polymer OSCs with improved performance over BHJ counterparts using a PM6 donor and different polymer acceptors, namely PYF-T-*o* and PYT.[180] The active layers were prepared with different solvents, such as tolune, aromatic hydrocarbons

without the aid of CF. The inadequate swelling issue of toluene was controlled by the addition of some solvent additive during the bottom and top layers deposition. The toluene-processed sequential processing improved the electron mobility to 3.3 times that of CF-processed LBL OSC and 2.4 times than that of the BHJ device, maintaining a balance between the e^{-}/h^{+} mobility. Thus, the toluene-processed LBL OSC achieved a PCE of 15.8%, while the BHJ OSC achieved a PCE of 14.2%. The morphological investigations suggested higher exciton generation in the bottom layer and increased electron mobility that improved the difficulty of long-distance electron transport to the cathode leading to enhancement in J_{SC} and FF.

Cao *et al.* synthesized a polymer donor PBQx-H-TF and polymer acceptor PYSe, which were implemented in bilayer OSCs using orthogonal solvents.[181] The corresponding quasi-planar heterojunction (Q-PHJ) all-polymer OSCs achieved a PCE of 15.77% that was higher than the BHJ counterpart (13.91%). The enhancement was attributed to the improved charge carrier transport and suppressed recombination. Benefiting from the Q-PHJ morphology, the device stability increased significantly compared to the BHJ counterpart. An all-polymer OSC prepared by LBL deposition improved the swelling of polymer films and promoted exciton dissociation and charge

transport with the reduction of trap-assisted recombination.[182] The polymer donor (PM6) was processed from CB and the acceptor (L15) was treated from CF with a trace of 1-CN as the additive to control the film microstructure and vertical distribution. The LBL OSC reached a high PCE of 16.15% that was higher than that for the BHJ counterpart (15.2%).

Zhao, *et al.* fabricated LBL all-polymer OSCs using PM6 as the donor and PY-V-γ polymer as the acceptor using toluene as the processing solvent and achieved a PCE of about 17% that was higher than the BHJ counterpart (16.3%), attributing to the improved vertical phase segregation, reduced charge carrier recombination and balanced charge transport.[183]

In summary, for all-polymer OSCs the polymer morphology in the active layer could be efficiently controlled by LBL processing leading to efficient and stable devices. This led to the optimized vertical phase separation as well as polymer microstructures formation in LBL-processed OSCs compared with that in BHJ films.

4. LBL-processed semitransparent OSCs

Because of the tunable absorption and high molar absorptivity of organic photoactive materials it is possible to fabricate semitransparent OSCs for various applications, like building-integrated photovoltaic (BIPV) windows, power windows, and green house applications.[184] Thus, the glass windows in buildings can be simultaneously used for electricity production and show an aesthetic appearance due to variable color transparency. In BHJ, lowering the composition of donor materials that absorb in the visible region to improve the average visible transparency (AVT) can impair the exciton dissociation and charge transport and thus decrease the device PCE. While, in LBL processing a thin layer of wide- or medium-bandgap donor material along with a thick layer of low bandgap acceptor can reduce the light absorption in the visible region still maintaining high exciton dissociation and charge transport properties to achieve enhancement in the AVT and PCE of the device along with its stability.

Song *et al.* prepared semitransparent OSCs using a sequentially deposited bilayer with PTB7-Th/IEICO-4F and attained a PCE of 8.5% with an AVT of around 21.5% which was higher compared to the BHJ counterpart (8.1%, AVT = 21.1%) (Fig. 16, Table 7).[185] Xue *et al.* reported a semitransparent OSC prepared by sequential deposition of PM6 and Y6 layers achieving a PCE of 12.6% at an AVT of 25.4%, while the ST-OSCs prepared with BHJ attained a PCE of 11.8% and an AVT of 22.9%.[186]

Wang *et al.* fabricated a PBDB-TF/Y6 based LBL ST-OSC in which the diffusion of the Y6 molecule occurred at the interface forming a p–i–n structure providing the best PCE of 12.9% and AVT of 14.5%.[187] A thickness dependent study further revealed the superiority of the LBL method over BHJ structures. Yang *et al.* developed ST-OSCs by sequential depositing of the PM6 donor and FFA BTP-eC9 and attained a PCE of 13.3% with an AVT of 18.5% and light utilization efficiency (LUE) of 2.46%.[188] The optimized opaque device achieved a PCE of 18.5%. Moreover, by instituting an efficient anti-reflective coating (ARC) layer, the AVT of ST-OSCs was significantly improved to 27.8% while still maintaining a PCE of 13.1%, along with the impressive LUE of 3.64% and color-rendering index (CRI) of 94.6%.

Huang *et al.* investigated the effect of molecular weight on the LBL OSCs that enabled ST-OSCs with a LUE of over 5% without complex optical engineering.[189] The device with different molecular weights of the PCE10-2F donor along with Y6 as the acceptor achieved PCEs ranging from 11.11–10.01% with a high AVT of 39.93-50.05%. The opaque device based on PCE10-2F/Y6 achieved an overall PCE of 14.53%. Thus, it is possible to develop efficient ST-OSCs with a high AVT using an LBL deposition technique with high morphological control.

Fig. 16 (a) Transmittance spectra of BHJ and bilayer LBL OSC. (b) Normalized thin film absorption spectra of PTB7-Th and IEICO-4F. (c) Photographs of the reference and bilayer ST-OSCs. Reprinted with permission from ref. 185. Copyright 2020, American Chemical Society.

An LBL-processed ST-OSC using the D18/N3 layer demonstrated a visible transparency of about 52% from the 400–740 nm region. By varying the thickness of the Ag layer from 10 to 20 nm and optimizing the donor layer the devices generated PCEs from 12.58% to 14.85% with an AVT of 22.81% to 9.48%.[190] Lunt and co-workers used an LBL approach and demonstrated ST-OSCs with a PCE of 8.8%, AVT of 40.9%, and a LUE of 3.6%.[191] The device exhibited exciton diffusion lengths >100 nm for both the polymer donor and IEICO-4F acceptor.

Here we have shown that the LBL deposition of D and A materials is a viable approach to enhance the efficiency and stability of ST-OSCs along with its AVT. This technique also allows us to adjust the film thickness and transparency because of the independent deposition of D and A layers, and the desired optical properties of both the photoactive materials.

5. Stability of LBL-processed OSCs

The major barrier for commercialization of OSCs is their poor stability. The stability of the OSCs mainly depends on factors like processing conditions, treatments during active layer deposition,

Table 7 Solar cell data for the BHJ and LBL-processed semitransparent OSCs

Active layer	Processing method	V_{OC} [V]	J_{SC} [mA cm^{-2}]	FF	PCE [%]	Ref.
PTB7-Th/IEICO-4F	LBL	0.67	19.60	0.65	8.50	185
PTB7-Th:IEICO-4F	BHJ	0.69	18.90	0.61	8.10	
PM6/Y6	LBL	0.83	21.40	0.70	12.60	186
PM6:Y6	BHJ	0.83	21.10	0.67	11.80	
PBDB-T-2F/Y6	LBL	0.84	22.51	0.68	12.91	187
PBDB-T-2F:Y6	BHJ	0.84	22.62	0.67	12.77	
PM6/BTP-eC9	LBL	0.82	22.50	0.72	13.30	188
PCE10-2F/Y6	LBL	0.78	20.37	0.69	11.11	189
D18/N3	LBL	0.85	23.14	0.76	14.85	190
PTB7-Th/IEICO-4F	LBL	0.70	19.80	0.63	8.80	191

contact with oxygen, water, and irradiation. The morphology control of the BHJ devices is extremely difficult leading to poor long-term stability under light/thermal soaking conditions.[192,193] A delicate balance between domain size, purity, and miscibility is required to attain a stable morphology. In PCBM-based devices, the oxidation of PCBM derivatives led to lowering of the LUMO energy level and thus acting as traps for electrons in the PCBM domain.[194] In BHJ devices the lateral phase separation led to aggregation with time and penetration of the A to the D phase and reduced the device morphology and stability. In contrast, the new technology based on LBL-processed p–i–n type OSCs shows excellent stability due to vertical phase separation.[100] This is mostly applicable to crystalline polymers which form robust ordered film at the nanoscale, so the acceptor can only penetrate to the amorphous region of the polymer film without affecting the crystallinity. It has been shown that in comparison to non-annealed devices, pre-annealing of the active layer significantly enhanced the stability. LBL OSCs showed almost no change in PCE, whereas 76% reduction was reported for the BHJ devices.[99] Therefore, LBL-processed OSCs have better control over the crystallinity and morphology forming order packing with high domain purity.

The PM6/IT-4F based LBL OSCs (0.04 cm^2) prepared by either spin-coating or doctor-blade coating using halogen-free solvent attained PCEs of 12.9 and 12.3%, respectively. For large area LBL OSCs device with 1 cm^2 cell size prepared by blade-coating a PCE of 11.4% was reported, which maintained high stability as the acceptor layer was protected from light by lying behind the donor layer.[195] The protection of the acceptor layer along with vertical component distribution was found to be a major advantage for the stability of LBL OSCs. This was also shown using a blade-coated J71/ITC6-IC device which retained 85% of the initial PCE (11.47%) compared to 68% retention for the BHJ device (10.41%).[196] The LBL OSCs showed greater stability than the BHJ device under illumination, thermal stress and bending cycle (Fig. 17).
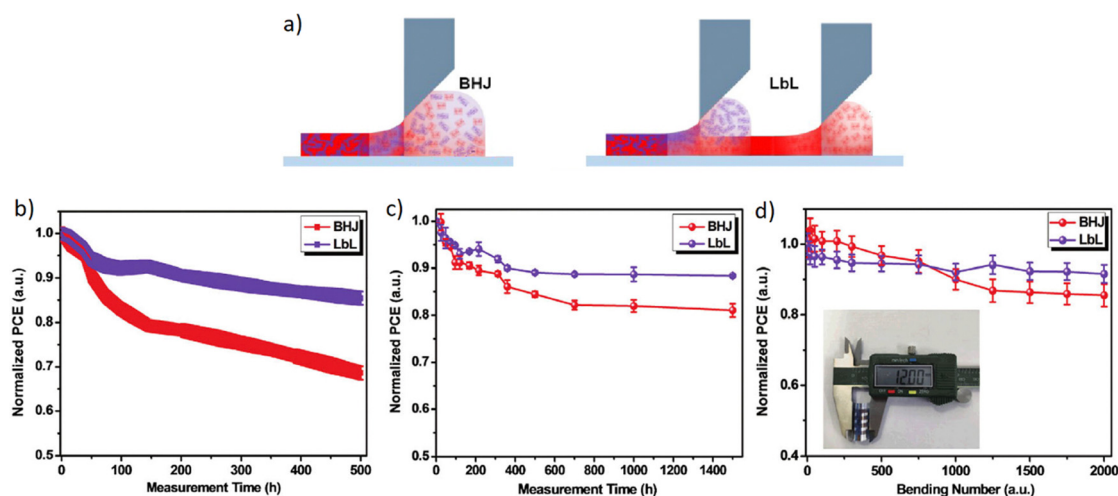

Fig. 17 (a) Schematic presentation of the BHJ and LBL film of the J71 donor and ITC6-IC acceptor preparation by blade coating. Variation of normalized average PCE losses over illumination time (b) under illumination, (c) thermal stress, and (d) bending stability for the BHJ and LbL OSCs. Reprinted with permission from ref. 196. Copyright 2019, Royal Society of Chemistry.

Recently, Kim and co-workers addressed the improved stability of LBL OSCs prepared using PTB7-Th as the donor and IEICO-4F as the acceptor along with 1,8-dibromooctane (DBO) as a cross-linking additive.[197] The irradiation of PTB7-Th + DBO film under UV light formed a photo-crosslinked polymer layer which improved the polymer crystallinity and glass transition temperature. The residual additive and non-crosslinked polymer were washed with CB. The device with the crosslinked polymer layer seems to improve both the thermal and light-soaking stability test. The same group demonstrated enhanced thermal stability of LBL OSCs by using 1-CN + DCM as a quasi-orthogonal solvent for the deposition of the Y6 acceptor layer.[198] This solvent mixture had a lower vapor pressure, which facilitated the dissolution and diffusion of the Y6 into the PM6 donor layer without compromising its film quality. The crystallinity of the BHJ interlayer increased in the donor domain resulting in a PCE of 14.1% with high thermal stability. The change in the film morphology was also investigated by absorption studies, which showed significant change in absorption for the BHJ blend compared to the LBL film, further suggesting its stability during thermal stress.

Fu *et al.* demonstrated excellent stability of all-polymer D18/PY-FY-based LBL devices retaining over 90% of their initial PCEs after annealing at 65 °C for 1300 h validating the advantage of LBL processing.[174] All polymer OSCs employing PBQx-H-TF/PBTIC-γ-TSe formed Q-PHJ demonstrating enhanced light and long-term stability retaining 80% (870 h) of its initial PCE compared to 70% (260 h) retention for the BHJ devices which is related to the better morphology of the LBL processed active layer.[181] Min and co-workers revealed enhanced mechanical stability of the LBL layers compared to the BHJ blend that was related to better molecular ordering and optimal vertical phase morphology.[177]

Thus, these studies demonstrated that the LBL approach is an excellent strategy to construct stable OSCs due to control of molecular crystallinity, ordering, domain control by choice of orthogonal solvents and finally vertical component distributions along with good surface homogeneity. Therefore they show potential over the BHJ counterpart for future applications. However, more efforts and studies are required to understand the morphology control to take the device from the laboratory scale to large area fabrications.

6. Summary and future prospects

In this review, we have described the recent progress in OSCs using polymer donors and fullerene/FFAs processed using the LBL technique. LBL deposition aims to achieve an optimal p–i–n structure for the active layer, which offers adequate D/A interfaces for exciton splitting and uniform channels for charge transport (electrons in the acceptor phase and holes in the donor phase) and extraction to reduce the charge recombination, which is helpful to realize high efficiency devices. One of the challenges in BHJ OSCs is to control the film morphology, which affects the performance and stability of the devices.

While the LBL processing solves the miscibility problem when depositing individual layers, broadening of the absorption spectrum, cascading the energy levels, and improving the charge carrier mobility. Unlike the BHJ active layer, the LBL method can produce separate D and A layers on the top and bottom of the BHJ layer. These layers have specific molecular orientation and arrangement in their pure phases. This enhances the morphological stability by increasing the crystallinity and reducing the rapid change in polymers' conformation. This also allows for precise control over the thickness and composition of each layer with preferred vertical components distribution, enabling better control over the active layer's morphology resulting in improved charge transport and collection. These morphological advantages lead to lower energy loss and improved thermal and mechanical stability in LBL devices. With the excellent advances in polymer donors and fullerene-free acceptors, the PCEs of the LBL-processed OSCs have reached over 19% which is comparable or even higher than BHJ counterparts. Table 8 compiles a summary of the selected best-performing D/A materials that reached PCEs over 18% by using LBL-processing.

Conjugated polymers with a pre-aggregation tendency have significant impact on the thin film morphology and is advantageous in LBL OSCs. The aggregated polymer film can regulate the film formation of the upper acceptor layer resulting in a quasi-planar heterojunction network structure with vertical phase separation for charge transport. One of the possible ways to enhance the efficiency of LBL OSCs is to explore new materials for the sequential deposition. By designing and synthesizing small molecules/polymers with desirable properties, such as strong absorption, good charge transport, and stable morphology, the performance of LBL OSCs could be significantly improved. Another key factor for improving the performance of LBL OSCs is the control of vertical phase separation within the active layer. This can be achieved by using appropriate solvents that have different degrees of compatibility with the D and A materials (orthogonal or even semi-orthogonal solvents), adding processing additives that can modify the interfacial properties, applying post treatments such as thermal annealing or solvent vapor annealing that can enhance the packing and morphology, and using a protecting solvent to prevent the dissolution of the bottom layers.

The field of LBL OSCs has advanced rapidly and achieved remarkable PCEs in both small-scale devices and large-scale modules. The p–i–n configuration formed by the LBL method has enabled the fabrication of large-area OSCs using a blade coating technique achieving a PCE over 11%, which is advantageous for roll-to-roll (R2R) processing. Despite the advances in LBL based OSCs, there are still some challenges that need to be addressed in future research to enhance their performance and stability.

(i) Recent research has suggested that one possible way to achieve p–i–n film morphology in LBL is the careful selection of solvents, co-solvents, and additives. However, most of these methods rely on practices and optimizations. Therefore, a standardized theoretical model based on machine learning

Table 8 Solar cell data of selected "champion" D/A materials prepared by LBL processing showing PCEs above 18%

Type	Device structure	Processing method	$D_{Solvent}/A_{Solvent}$	V_{OC} [V]	J_{SC} [mA cm^{-2}]	FF	PCE [%]	Ref.
Binary	ITO/PEDOT:PSS/PM6:P-Cl/BTP-eC9:P-Cl/PNDIT-F3N/Ag	LBL SC[a]	CB/CF	0.85	27.81	0.80	19.10	73
	ITO/PEDOT:PSS/D18/L8-BO/PDIN/Ag	LBL SC	CF/CF	0.91	26.86	0.77	19.05	128
	ITO/PEDOT:PSS/PM6:FA-C1/L8-BO/PDINN/Ag	LBL SC	CF/CF	0.88	26.68	0.81	19.02	138
Ternary	ITO/PEDOT:PSS/D18/3-BTP-ThCl:BTP-Th (2-CN)/PDINOH/Ag	LBL SC	CB/CF	0.86	28.16	0.79	19.15	159
Multicomponent	ITO/PEDOT:PSS/D18-Cl:BTP-eC9/PM6:L8-BO/PNDIT-F3N/Ag	LBL SC	CF/CF	0.89	27.02	0.80	19.61	72
All-polymer	ITO/PEDOT:PSS/PM6/PYSSe-V:PY-Cl/PFN-Br/Ag	LBL SC	CF/CF	0.91	25.88	0.77	18.14	179

[a] SC: spin coating.

must be developed to study the dependence of film morphology on processing conditions.

(ii) The LBL processed OSCs exhibit better vertical phase distribution and morphological features than the BHJ devices. However, the current understanding of these characteristics, such as molecular crystallinity, component distribution, and orientation of molecules requires further investigations. More experimental and theoretical studies are needed to elucidate the relationship between morphology and molecular functionality.

(iii) A major challenge for LBL OSCs is the use of halogenated solvents, which are harmful to the environment. To make LBL OSCs suitable for mass production, new D and A materials with high solubility in eco-friendly solvents need to be developed. At the same time, the choice of solvents and additives are also important for optimization of the morphology.

(iv) Most of the LBL devices are based on the conventional structure where the A layer is deposited over the D layer. However, there are hardly any reports on LBL OSCs with an inverted structure in which the D layer is coated over the A layer. This is mainly due to the dissolution of NFAs during the sequential deposition of the polymer donor above the NFAs. Therefore, it is important to find appropriate molecular systems and new processing methods to fabricate inverted devices.

(v) To commercialize LBL technology, various roll-to-roll (R2R) techniques, such as slot-die coating, blade coating, and ink-jet printing methods need to be explored. These techniques have been successfully implemented in the lab but require further investigation for industrial applications.

(vi) Although the LBL processed device attained better performance as compared to the BHJ counterpart, more systematic investigations are required on the operational device stability to ensure the practical viability of LBL OSCs in the future.

(vii) In recent years, it has been reported that solid additives can be used to improve the stability of BHJ-based OSCs. We also recommend that these additives can be utilized in LBL concepts to further improve the stability of the OSCs.

It has been reported that under low light conditions the dark current is minimized in LBL OSCs with reduced trap-assisted recombination, thus improving the FF. This could be advantageous for the p–i–n-type LBL OSCs for use in indoor applications. In summary, LBL OSCs offer several advantages over conventional BHJ devices, including tunable morphology, enhanced efficiency, improved stability, and the potential for low-cost manufacturing. While challenges still exist in their development, LBL OSCs represent a promising alternative for the future of efficient and stable solar cells, contributing to the broader goal of clean and renewable energy.

Conflicts of interest

There are no conflicts to declare.

Acknowledgements

References

1 L. Lu, T. Zheng, Q. Wu, A. M. Schneider, D. Zhao and L. Yu, *Chem. Rev.*, 2015, **115**, 12666–12731.

2 H. Yao, L. Ye, H. Zhang, S. Li, S. Zhang and J. Hou, *Chem. Rev.*, 2016, **116**, 7397–7457.

3 A. Mishra, *Energy Environ. Sci.*, 2020, **13**, 4738–4793.

4 G. Zhang, F. R. Lin, F. Qi, T. Heumüller, A. Distler, H.-J. Egelhaaf, N. Li, P. C. Y. Chow, C. J. Brabec, A. K. Y. Jen and H.-L. Yip, *Chem. Rev.*, 2022, **18**, 14180–14274.

5 A. Mishra and G. D. Sharma, *Angew. Chem., Int. Ed.*, 2023, **62**, e202219245.

6 P. Cheng and Y. Yang, *Acc. Chem. Res.*, 2020, **53**, 1218–1228.

7 S. Dong, T. Jia, K. Zhang, J. Jing and F. Huang, *Joule*, 2020, **4**, 2004–2016.

8 Y. Liu, B. Liu, C.-Q. Ma, F. Huang, G. Feng, H. Chen, J. Hou, L. Yan, Q. Wei, Q. Luo, Q. Bao, W. Ma, W. Liu, W. Li, X. Wan, X. Hu, Y. Han, Y. Li, Y. Zhou, Y. Zou, Y. Chen, Y. Liu, L. Meng, Y. Li, Y. Chen, Z. Tang, Z. Hu, Z.-G. Zhang and Z. Bo, *Sci. China: Chem.*, 2022, **65**, 1457–1497.

9 G. Wang, M. A. Adil, J. Zhang and Z. Wei, *Adv. Mater.*, 2019, **31**, 1805089.

10 P. Xue, P. Cheng, R. P. S. Han and X. Zhan, *Mater. Horiz.*, 2021, **9**, 194–219.

11 G. A. Chamberlain, *Sol. Cells*, 1983, **8**, 47–83.

12 O. V. Mikhnenko, P. W. M. Blom and T.-Q. Nguyen, *Energy Environ. Sci.*, 2015, **8**, 1867–1888.

13 S. Giannini, W.-T. Peng, L. Cupellini, D. Padula, A. Carof and J. Blumberger, *Nat. Commun.*, 2022, **13**, 2755.

14 C. W. Tang, *Appl. Phys. Lett.*, 1986, **48**, 183–185.

15 R. R. Lunt, N. C. Giebink, A. A. Belak, J. B. Benziger and S. R. Forrest, *J. Appl. Phys.*, 2009, **105**, 053711–053717.

16 M. Hiramoto, H. Fujiwara and M. Yokoyama, *Appl. Phys. Lett.*, 1991, **58**, 1062–1064.

17 M. Hiramoto, H. Fujiwara and M. Yokoyama, *J. Appl. Phys.*, 1992, **72**, 3781–3787.

18 N. S. Sariciftci, L. Smilowitz, A. J. Heeger and F. Wudl, *Science*, 1992, **258**, 1474–1476.

19 G. Yu, J. Gao, J. C. Hummelen, F. Wudl and A. J. Heeger, *Science*, 1995, **270**, 1789–1791.

20 C. J. Brabec, N. S. Sariciftci and J. C. Hummelen, *Adv. Funct. Mater.*, 2001, **11**, 15–26.

21 Y. He and Y. Li, *Phys. Chem. Chem. Phys.*, 2011, **13**, 1970–1983.

22 C.-Z. Li, H.-L. Yip and A. K. Y. Jen, *J. Mater. Chem.*, 2012, **22**, 4161–4177.

23 T. Liu and A. Troisi, *Adv. Mater.*, 2013, **25**, 1038–1041.

24 F. Zhang, O. Inganäs, Y. Zhou and K. Vandewal, *Natl. Sci. Rev.*, 2016, **3**, 222–239.

25 Z. Li, E. Speller, J. Durrant, J.-S. Kim, W. Tsoi, A. J. Clarke, J. Luke, T. Wang, H. C. Wong, H. Lee and N. Li, *J. Mater. Chem. A*, 2019, **7**, 23361–23377.

26 Y.-Y. Lai, Y.-J. Cheng and C. S. Hsu, *Energy Environ. Sci.*, 2014, **7**, 1866–1883.

27 J. Zhao, Y. Li, G. Yang, K. Jiang, H. Lin, H. Ade, W. Ma and H. Yan, *Nat. Energy*, 2016, **1**, 15027.

28 D. Deng, Y. Zhang, J. Zhang, Z. Wang, L. Zhu, J. Fang, B. Xia, Z. Wang, K. Lu, W. Ma and Z. Wei, *Nat. Commun.*, 2016, **7**, 13740.

29 G. Zhang, J. Zhao, P. C. Y. Chow, K. Jiang, J. Zhang, Z. Zhu, J. Zhang, F. Huang and H. Yan, *Chem. Rev.*, 2018, **118**, 3447–3507.

30 Y. Lin, J. Wang, Z.-G. Zhang, H. Bai, Y. Li, D. Zhu and X. Zhan, *Adv. Mater.*, 2015, **27**, 1170–1174.

31 J. Yuan, Y. Zhang, L. Zhou, G. Zhang, H.-L. Yip, T.-K. Lau, X. Lu, C. Zhu, H. Peng, P. A. Johnson, M. Leclerc, Y. Cao, J. Ulanski, Y. Li and Y. Zou, *Joule*, 2019, **3**, 1140–1151.

32 Q. Yue, W. Liu and X. Zhu, *J. Am. Chem. Soc.*, 2020, **142**, 11613–11628.

33 S. Li, C.-Z. Li, M. Shi and H. Chen, *ACS Energy Lett.*, 2020, **5**, 1554–1567.

34 C. Li, J. Zhou, J. Song, J. Xu, H. Zhang, X. Zhang, J. Guo, L. Zhu, D. Wei, G. Han, J. Min, Y. Zhang, Z. Xie, Y. Yi, H. Yan, F. Gao, F. Liu and Y. Sun, *Nat. Energy*, 2021, **6**, 605–613.

35 R. Sun, Y. Wu, X. Yang, Y. Gao, Z. Chen, K. Li, J. Qiao, T. Wang, J. Guo, C. Liu, X. Hao, H. Zhu and J. Min, *Adv. Mater.*, 2022, **34**, 2110147.

36 C. He, Y. Pan, Y. Ouyang, Q. Shen, Y. Gao, K. Yan, J. Fang, Y. Chen, C.-Q. Ma, J. Min, C. Zhang, L. Zuo and H. Chen, *Energy Environ. Sci.*, 2022, **15**, 2537–2544.

37 L. Zhu, M. Zhang, J. Xu, C. Li, J. Yan, G. Zhou, W. Zhong, T. Hao, J. Song, X. Xue, Z. Zhou, R. Zeng, H. Zhu,

C.-C. Chen, R. C. I. MacKenzie, Y. Zou, J. Nelson, Y. Zhang, Y. Sun and F. Liu, *Nat. Mater.*, 2022, **21**, 656–663.

38 K. Chong, X. Xu, H. Meng, J. Xue, L. Yu, W. Ma and Q. Peng, *Adv. Mater.*, 2022, **34**, 2109516.

39 Z. Zheng, J. Wang, P. Bi, J. Ren, Y. Wang, Y. Yang, X. Liu, S. Zhang and J. Hou, *Joule*, 2022, **6**, 171–184.

40 J. Wang, Z. Zheng, P. Bi, Z. Chen, Y. Wang, X. Liu, S. Zhang, X. Hao, M. Zhang, Y. Li and J. Hou, *Natl. Sci. Rev.*, 2023, **10**, nwad085.

41 S. Chandrabose, K. Chen, A. J. Barker, J. J. Sutton, S. K. K. Prasad, J. Zhu, J. Zhou, K. C. Gordon, Z. Xie, X. Zhan and J. M. Hodgkiss, *J. Am. Chem. Soc.*, 2019, **141**, 6922–6929.

42 H. Chen, T. Zhao, L. Li, P. Tan, H. Lai, Y. Zhu, X. Lai, L. Han, N. Zheng, L. Guo and F. He, *Adv. Mater.*, 2021, **33**, 2102778.

43 M. T. Sajjad, A. Ruseckas, L. K. Jagadamma, Y. Zhang and I. D. W. Samuel, *J. Mater. Chem. A*, 2020, **8**, 15687–15694.

44 Y. Firdaus, V. M. L. Corre, S. Karuthedath, W. Liu, A. Markina, W. Huang, S. Chattopadhyay, M. M. Nahid, M. I. Nugraha, Y. Lin, A. Seitkhan, A. Basu, W. Zhang, I. McCulloch, H. Ade, J. Labram, F. Laquai, D. Andrienko, L. J. A. Koster and T. D. Anthopoulos, *Nat. Commun.*, 2020, **11**, 5220.

45 S. Y. Park, S. Chandrabose, M. B. Price, H. S. Ryu, T. H. Lee, Y. S. Shin, Z. Wu, W. Lee, K. Chen, S. Dai, J. Zhu, P. Xue, X. Zhan, H. Y. Woo, J. Y. Kim and J. M. Hodgkiss, *Nano Energy*, 2021, **84**, 105924.

46 M. Riede, D. Spoltore and K. Leo, *Adv. Energy Mater.*, 2021, **11**, 2002653.

47 F. Qin, L. Sun, H. Chen, Y. Liu, X. Lu, W. Wang, T. Liu, X. Dong, P. Jiang, Y. Jiang, L. Wang and Y. Zhou, *Adv. Mater.*, 2021, **33**, 2103017.

48 X. Dong, Y. Jiang, L. Sun, F. Qin, X. Zhou, X. Lu, W. Wang and Y. Zhou, *Adv. Funct. Mater.*, 2022, **32**, 2110209.

49 B. Kan, F. Ershad, Z. Rao and C. Yu, *Nano Res.*, 2021, **14**, 2891–2903.

50 C. Liu, C. Xiao, C. Xie and W. Li, *Nano Energy*, 2021, **89**, 106399.

51 M. Moser, A. Wadsworth, N. Gasparini and I. McCulloch, *Adv. Energy Mater.*, 2021, **11**, 2100056.

52 C. J. Brabec, M. Heeney, I. McCulloch and J. Nelson, *Chem. Soc. Rev.*, 2011, **40**, 1185–1199.

53 Y. Huang, E. J. Kramer, A. J. Heeger and G. C. Bazan, *Chem. Rev.*, 2014, **114**, 7006–7043.

54 Y. Yu, R. Sun, T. Wang, X. Yuan, Y. Wu, Q. Wu, M. Shi, W. Yang, X. Jiao and J. Min, *Adv. Funct. Mater.*, 2021, **31**, 2008767.

55 M. Gao, W. Wang, J. Hou and L. Ye, *Aggregate*, 2021, **2**, e46.

56 G. Schulz, M. Lobert, I. Ata, M. Urdanpilleta, M. Lindén, A. Mishra and P. Bäuerle, *J. Mater. Chem. A*, 2015, **3**, 13738–13748.

57 Z. Shi, H. Liu, Y. Wang, J. Li, Y. Bai, F. Wang, X. Bian, T. Hayat, A. Alsaedi and Z. A. Tan, *ACS Appl. Mater. Interfaces*, 2017, **9**, 43871–43879.

58 H. Dahiya, R. Suthar, K. Khandelwal, S. Karak and G. D. Sharma, *ACS Appl. Electron. Mater.*, 2022, **4**, 5119–5143.

59 Y. Wang, J. Lee, X. Hou, C. Labanti, J. Yan, E. Mazzolini, A. Parhar, J. Nelson, J.-S. Kim and Z. Li, *Adv. Energy Mater.*, 2021, **11**, 2003002.

60 F. Zhao, H. Zhang, R. Zhang, J. Yuan, D. He, Y. Zou and F. Gao, *Adv. Energy Mater.*, 2020, **10**, 2002746.

61 Y. Yao, J. Hou, Z. Xu, G. Li and Y. Yang, *Adv. Funct. Mater.*, 2008, **18**, 1783–1789.

62 T. H. Lee, S. Y. Park, X. Du, S. Park, K. Zhang, N. Li, S. Cho, C. J. Brabec and J. Y. Kim, *ACS Appl. Mater. Interfaces*, 2020, **12**, 55945–55953.

63 S. Inaba and V. Vohra, *Materials*, 2017, **10**, 518.

64 X. Li, X. Du, J. Zhao, H. Lin, C. Zheng and S. Tao, *Sol. RRL*, 2021, **5**, 2000592.

65 M. H. Jee, H. S. Ryu, D. Lee, W. Lee and H. Y. Woo, *Adv. Sci.*, 2022, **9**, 2201876.

66 R. Yu, X. Wei, G. Wu and Z. A. Tan, *Aggregate*, 2022, **3**, e107.

67 M. D. M. Faure and B. H. Lessard, *J. Mater. Chem. C*, 2021, **9**, 14–40.

68 M. Li, Q. Wang, J. Liu, Y. Geng and L. Ye, *Mater. Chem. Front.*, 2021, **5**, 4851–4873.

69 S. Guo, Y. Hu, M. Qin, J. Li, Y. Wang, J. Qin and P. Cheng, *Mater. Horiz.*, 2022, **9**, 2097–2108.

70 J. Zhang, B. Kan, A. J. Pearson, A. J. Parnell, J. F. K. Cooper, X.-K. Liu, P. J. Conaghan, T. R. Hopper, Y. Wu, X. Wan, F. Gao, N. C. Greenham, A. A. Bakulin, Y. Chen and R. H. Friend, *J. Mater. Chem. A*, 2018, **6**, 18225–18233.

71 Y. Cui, S. Zhang, N. Liang, J. Kong, C. Yang, H. Yao, L. Ma and J. Hou, *Adv. Mater.*, 2018, **30**, 1802499.

72 X. Xu, W. Jing, H. Meng, Y. Guo, L. Yu, R. Li and Q. Peng, *Adv. Mater.*, 2023, **35**, 2208997.

73 M. Zhou, C. Liao, Y. Duan, X. Xu, L. Yu, R. Li and Q. Peng, *Adv. Mater.*, 2023, **35**, 2208279.

74 L. Hong, H. Yao, Y. Cui, P. Bi, T. Zhang, Y. Cheng, Y. Zu, J. Qin, R. Yu, Z. Ge and J. Hou, *Adv. Mater.*, 2021, **33**, 2103091.

75 L. Zhan, S. Li, X. Xia, Y. Li, X. Lu, L. Zuo, M. Shi and H. Chen, *Adv. Mater.*, 2021, **33**, 2007231.

76 X. Xu, L. Yu, H. Meng, L. Dai, H. Yan, R. Li and Q. Peng, *Adv. Funct. Mater.*, 2021, **32**, 2108797.

77 J. Chen, J. Cao, L. Liu, L. Xie, H. Zhou, J. Zhang, K. Zhang, M. Xiao and F. Huang, *Adv. Funct. Mater.*, 2022, **32**, 2200629.

78 R. Sun, Q. Wu, J. Guo, T. Wang, Y. Wu, B. Qiu, Z. Luo, W. Yang, Z. Hu, J. Guo, M. Shi, C. Yang, F. Huang, Y. Li and J. Min, *Joule*, 2020, **4**, 407–419.

79 B. Zhang, F. Yang, S. Chen, H. Chen, G. Zeng, Y. Shen, Y. Li and Y. Li, *Adv. Funct. Mater.*, 2022, **32**, 2202011.

80 H. Hoppe and N. S. Sariciftci, *J. Mater. Chem.*, 2006, **16**, 45–61.

81 S. Shoaee, M. Stolterfoht and D. Neher, *Adv. Energy Mater.*, 2018, **8**, 1703355.

82 K. H. Lee, P. E. Schwenn, A. R. G. Smith, H. Cavaye, P. E. Shaw, M. James, K. B. Krueger, I. R. Gentle, P. Meredith and P. L. Burn, *Adv. Mater.*, 2011, **23**, 766–770.

83 D. H. Wang, H. K. Lee, D.-G. Choi, J. H. Park and O. O. Park, *Appl. Phys. Lett.*, 2009, **95**, 043505.

84 A. L. Ayzner, C. J. Tassone, S. H. Tolbert and B. J. Schwartz, *J. Phys. Chem. C*, 2009, **113**, 20050–20060.

85 M. K. Wong and K. Y. Wong, *Synth. Met.*, 2013, **170**, 1–6.

86 X. Lin, J. Seok, S. Yoon, T. Kim, B. Kim and K. Kim, *Synth. Met.*, 2014, **196**, 145–150.

87 A. Loiudice, A. Rizzo, G. Latini, C. Nobile, M. D. Giorgi and G. Gigli, *Sol. Energy Mater. Sol. Cell*, 2012, **100**, 147–152.

88 G. Zhang, R. C. Huber, A. S. Ferreira, S. D. Boyd, C. K. Luscombe, S. H. Tolbert and B. J. Schwartz, *J. Phys. Chem. C*, 2014, **118**, 18424–18435.

89 H. Li, Y.-F. Li and J. Wang, *Appl. Phys. Lett.*, 2012, **101**, 033907.

90 H. Li and J. Wang, *Appl. Phys. Lett.*, 2012, **101**, 263901.

91 D. H. Wang, J. S. Moon, J. Seifter, J. Jo, J. H. Park, O. O. Park and A. J. Heeger, *Nano Lett.*, 2011, **11**, 3163–3168.

92 P. Cheng, J. Hou, Y. Li and X. Zhan, *Adv. Energy Mater.*, 2014, **4**, 1301349.

93 C. Lang, J. Fan, Y. Zhang, F. Guo and L. Zhao, *Org. Electron.*, 2016, **36**, 82–88.

94 J. C. Aguirre, S. A. Hawks, A. S. Ferreira, P. Yee, S. Subramaniyan, S. A. Jenekhe, S. H. Tolbert and B. J. Schwartz, *Adv. Energy Mater.*, 2015, **5**, 1402020.

95 Y. Liu, F. Liu, H.-W. Wang, D. Nordlund, Z. Sun, S. Ferdous and T. P. Russell, *ACS Appl. Mater. Interfaces*, 2015, **7**, 653–661.

96 J. J. van Franeker, S. Kouijzer, X. Lou, M. Turbiez, M. M. Wienk and R. A. J. Janssen, *Adv. Energy Mater.*, 2015, **5**, 1500464.

97 D. H. Kim, J. Mei, A. L. Ayzner, K. Schmidt, G. Giri, A. L. Appleton, M. F. Toney and Z. Bao, *Energy Environ. Sci.*, 2014, **7**, 1103–1109.

98 Y. Shimata, M. Ide, M. Tashiro, M. Katouda, Y. Imamura and A. Saeki, *J. Phys. Chem. C*, 2016, **120**, 17887–17897.

99 P. Cheng, C. Yan, Y. Wu, S. Dai, W. Ma and X. Zhan, *J. Mater. Chem. C*, 2016, **4**, 8086–8093.

100 M. Kim, S. Park, D. Y. Ryu and K. Kim, *Polymer*, 2016, **103**, 132–139.

101 Y. Jang, Y. Ju Cho, M. Kim, J. Seok, H. Ahn and K. Kim, *Sci. Rep.*, 2017, **7**, 9690.

102 H. Hwang, H. Lee, S. Shafian, W. Lee, J. Seok, K. Y. Ryu, D. Yeol Ryu and K. Kim, *Polymers*, 2017, **9**, 456.

103 Q. Liao, B. Li, H. Sun, C. W. Koh, X. Zhang, B. Liu, H. Y. Woo and X. Guo, *Mater. Rep. Energy*, 2021, **1**, 100063.

104 J. Wang and X. Zhan, *Acc. Chem. Res.*, 2021, **54**, 132–143.

105 C. Zhu, J. Yuan, F. Cai, L. Meng, H. Zhang, H. Chen, J. Li, B. Qiu, H. Peng, S. Chen, Y. Hu, C. Yang, F. Gao, Y. Zou and Y. Li, *Energy Environ. Sci.*, 2021, **13**, 2459–2466.

106 A. S. Gertsen, M. F. Castro, R. R. Søndergaard and J. W. Andreasen, *Flexible Printed Electron.*, 2020, **5**, 014004.

107 W. Yang, W. Wang, Y. Wang, R. Sun, J. Guo, H. Li, M. Shi, J. Guo, Y. Wu, T. Wang, G. Lu, C. J. Brabec, Y. Li and J. Min, *Joule*, 2021, **5**, 1209–1230.

108 S. Park, T. Kim, S. Yoon, C. W. Koh, H. Y. Woo and H. J. Son, *Adv. Mater.*, 2020, **32**, 2002217.

109 G. Bernardo, T. Lopes, D. G. Lidzey and A. Mendes, *Adv. Energy Mater.*, 2021, **11**, 2100342.

110 L. Huang, P. Jiang, Y. Zhang, L. Zhang, Z. Yu, Q. He, W. Zhou, L. Tan and Y. Chen, *ACS Appl. Mater. Interfaces*, 2019, **11**, 26213–26221.

111 T. H. Lee, S. Y. Park, W.-W. Park, X. Du, J. H. Son, N. Li, O.-H. Kwon, H. Y. Woo, C. J. Brabec and J. Y. Kim, *ACS Energy Lett.*, 2020, **5**, 1628–1635.

112 R. Sun, J. Guo, C. Sun, T. Wang, Z. Luo, Z. Zhang, X. Jiao, W. Tang, C. Yang, Y. Li and J. Min, *Energy Environ. Sci.*, 2019, **12**, 384–395.

113 H. Huang, X. Li, C. Sun, I. Angunawela, B. Qiu, J. Du, S. Qin, L. Meng, Z. Zhang, H. Ade and Y. Li, *J. Mater. Chem. C*, 2020, **8**, 7718–7724.

114 L. Arunagiri, G. Zhang, H. Hu, H. Yao, K. Zhang, Y. Li, P. C. Y. Chow, H. Ade and H. Yan, *Adv. Funct. Mater.*, 2019, **29**, 1902478.

115 Q. He, W. Sheng, M. Zhang, G. Xu, P. Zhu, H. Zhang, Z. Yao, F. Gao, F. Liu, X. Liao and Y. Chen, *Adv. Energy Mater.*, 2021, **11**, 2003390.

116 L. Ye, Y. Xiong, Z. Chen, Q. Zhang, Z. Fei, R. Henry, M. Heeney, B. T. O'Connor, W. You and H. Ade, *Adv. Mater.*, 2019, **31**, 1808153.

117 Z. Lin, F. Du, H. Wang, J. Cao and W. Tang, *J. Mater. Chem. C*, 2022, **10**, 10511–10518.

118 H. Kang, X. Zhang, X. Xu, Y. Li, S. Li, Q. Cheng, L. Huang, Y. Jing, H. Zhou, Z. Ma and Y. Zhang, *J. Phys. Chem. Lett.*, 2021, **12**, 10663–10670.

119 J. Deng, S. Huang, J. Liu, D. Zhou, L. Zhao, L. Liu, B. Huang, Y. Cheng, C. Yang, F. Wu and L. Chen, *Chem. Eng. J.*, 2022, **443**, 136515.

120 S. Liu, Y. Zhou, Z. Liang, B. Zhao, W. Wang, Z. Xue, K. Ding, Z. Cong, H. Wu, G. Lu and C. Gao, *ACS Appl. Energy Mater.*, 2023, **6**, 5047–5057.

121 H. Ning, Q. Jiang, P. Han, M. Lin, G. Zhang, J. Chen, H. Chen, S. Zeng, J. Gao, J. Liu, F. He and Q. Wu, *Energy Environ. Sci.*, 2021, **14**, 5919–5928.

122 X. Liang, S. Zhang, Y. Wu, J. Wang, C. Yang, A. Saparbaev, S. Wen and X. Bao, *Org. Electron.*, 2022, **107**, 106560.

123 J. Wan, L. Zeng, X. Liao, Z. Chen, S. Liu, P. Zhu, H. Zhu and Y. Chen, *Adv. Funct. Mater.*, 2022, **32**, 2107567.

124 X. Li, L. Cao, X. Yu, X. Du, H. Lin, G. Yang, Z. Chen, C. Zheng and S. Tao, *Sol. RRL*, 2022, **6**, 2200076.

125 W. Gao, F. Qi, Z. Peng, F. R. Lin, K. Jiang, C. Zhong, W. Kaminsky, Z. Guan, C.-S. Lee, T. J. Marks, H. Ade and A. K. Y. Jen, *Adv. Mater.*, 2022, **34**, 2202089.

126 C. He, Y. Pan, G. Lu, B. Wu, X. Xia, C.-Q. Ma, Z. Chen, H. Zhu, X. Lu, W. Ma, L. Zuo and H. Chen, *Adv. Mater.*, 2022, **34**, 2203379.

127 Z. Zhao, J. Zhao, S. Chung, K. Cho, W. Xu and Z. Kan, *ACS Mater. Lett.*, 2023, **5**, 1718–1726.

128 Y. Wei, Z. Chen, G. Lu, N. Yu, C. Li, J. Gao, X. Gu, X. Hao, G. Lu, Z. Tang, J. Zhang, Z. Wei, X. Zhang and H. Huang, *Adv. Mater.*, 2022, **34**, 2204718.

129 X. Wu, X. Wu, S. Peng, L. Xiao, Z. Xiao, W. Zhang, G. Ren, Y. Min and Y. Liu, *Sol. RRL*, 2023, **7**, 2300136.

130 K. Weng, L. Ye, L. Zhu, J. Xu, J. Zhou, X. Feng, G. Lu, S. Tan, F. Liu and Y. Sun, *Nat. Commun.*, 2020, **11**, 2855.

131 H. Fu, W. Gao, Y. Li, F. Lin, X. Wu, J. H. Son, J. Luo, H. Y. Woo, Z. Zhu and A. K. Y. Jen, *Small Methods*, 2020, **4**, 2000687.

132 S. Karuthedath, Y. Firdaus, A. D. Scaccabarozzi, M. I. Nugraha, S. Alam, T. D. Anthopoulos and F. Laquai, *Small Struct.*, 2022, **3**, 2100199.

133 Q. Li, L.-M. Wang, S. Liu, L. Guo, S. Dong, G. Ma, Z. Cao, X. Zhan, X. Gu, T. Zhu, Y.-P. Cai and F. Huang, *ACS Energy Lett.*, 2020, **5**, 3637–3646.

134 X. Ma, Q. Jiang, W. Xu, C. Xu, S. Young Jeong, H. Young Woo, Q. Wu, X. Zhang, G. Yuan and F. Zhang, *Chem. Eng. J.*, 2022, **442**, 136368.

135 X. Li, R. Zhu, Z. He, X. Du, H. Lin, C. Zheng, G. Yang, Z. Chen and S. Tao, *ACS Appl. Mater. Interfaces*, 2022, **14**, 25842–25850.

136 W. Xu, X. Li, S. Y. Jeong, J. H. Son, Z. Zhou, Q. Jiang, H. Y. Woo, Q. Wu, X. Zhu, X. Ma and F. Zhang, *J. Mater. Chem. C*, 2022, **10**, 5489–5496.

137 Y. Wei, J. Yu, L. Qin, H. Chen, X. Wu, Z. Wei, X. Zhang, Z. Xiao, L. Ding, F. Gao and H. Huang, *Energy Environ. Sci.*, 2021, **14**, 2314–2321.

138 G. Ding, T. Chen, M. Wang, X. Xia, C. He, X. Zheng, Y. Li, D. Zhou, X. Lu, L. Zuo, Z. Xu and H. Chen, *Nano-Micro Lett.*, 2023, **15**, 92.

139 Y. Wang, J. Xue, H. Zhong, C. R. Everett, X. Jiang, M. A. Reus, A. Chumakov, S. V. Roth, M. A. Adedeji, N. Jili, K. Zhou, G. Lu, Z. Tang, G. T. Mola, P. Muller-Buschbaum and W. Ma, *Adv. Energy Mater.*, 2023, **13**, 2203496.

140 Y. Yang, E. Feng, H. Li, Z. Shen, W. Liu, J. Guo, Q. Luo, J. Zhang, G. Lu, C. Ma and J. Yang, *Nano Res.*, 2021, **14**, 4236–4242.

141 P. Li, A. Hoff, A. Gasonoo, M. R. Niazi, M. Nazari and G. C. Welch, *Adv. Mater. Interfaces*, 2023, **10**, 2202156.

142 L. Xie, J. Zhang, W. Song, L. Hong, J. Ge, P. Wen, B. Tang, T. Wu, X. Zhang, Y. Li and Z. Ge, *ACS Appl. Mater. Interfaces*, 2021, **13**, 20405–20416.

143 A. Yi, S. Chae, H. Yoon and H. J. Kim, *ACS Appl. Mater. Interfaces*, 2021, **13**, 60288–60298.

144 Y. Cho, T. L. Nguyen, H. Oh, K. Y. Ryu, H. Y. Woo and K. Kim, *ACS Appl. Mater. Interfaces*, 2018, **10**, 27757–27763.

145 M. Ren, G. Zhang, Z. Chen, J. Xiao, X. Jiao, Y. Zou, H.-L. Yip and Y. Cao, *ACS Appl. Mater. Interfaces*, 2020, **12**, 13077–13086.

146 W. Xu, X. Ma, J. H. Son, S. Y. Jeong, L. Niu, C. Xu, S. Zhang, Z. Zhou, J. Gao, H. Y. Woo, J. Zhang, J. Wang and F. Zhang, *Small*, 2022, **18**, 2104215.

147 Y. Li, J. Wu, H. Tang, X. Yi, Z. Liu, Q. Yang, Y. Fu, J. Liu and Z. Xie, *ACS Appl. Mater. Interfaces*, 2022, **14**, 31054–31065.

148 R. Zhu, X. Li, L. Cao, X. Du, H. Lin, G. Yang, C. Zheng, Z. Chen and S. Tao, *Org. Electron.*, 2022, **111**, 106651.

149 T. Gokulnath, R. Durga Gayathri, H.-Y. Park, J. Kim, H. Kim, J. Kim, S. S. Reddy, J. Yoon and S.-H. Jin, *Chem. Eng. J.*, 2022, **448**, 137621.

150 Y. Cai, Q. Li, G. Lu, H. S. Ryu, Y. Li, H. Jin, Z. Chen, Z. Tang, G. Lu, X. Hao, H. Y. Woo, C. Zhang and Y. Sun, *Nat. Commun.*, 2022, **13**, 2369.

151 J. Han, H. Xu, S. H. K. Paleti, Y. Wen, J. Wang, Y. Wu, F. Bao, C. Yang, X. Li, X. Jian, J. Wang, S. Karuthedath, J. Gorenflot, F. Laquai, D. Baran and X. Bao, *ACS Energy Lett.*, 2022, **7**, 2927–2936.

152 K. Jiang, J. Zhang, Z. Peng, F. Lin, S. Wu, Z. Li, Y. Chen, H. Yan, H. Ade, Z. Zhu and A. K. Y. Jen, *Nat. Commun.*, 2021, **12**, 468.

153 R. R. Lunt, J. B. Benziger and S. R. Forrest, *Adv. Mater.*, 2010, **22**, 1233–1236.

154 J. Wang, S. Wen, J. Hu, J. Han, C. Yang, J. Li, X. Bao and S. Yan, *Chem. Eng. J.*, 2023, **452**, 139462.

155 X. Ma, W. Xu, Z. Liu, S. Y. Jeong, C. Xu, J. Zhang, H. Y. Woo, Z. Zhou and F. Zhang, *ACS Appl. Mater. Interfaces*, 2023, **15**, 7247–7254.

156 X. Li, H. Yang, X. Du, H. Lin, G. Yang, C. Zheng and S. Tao, *Chem. Eng. J.*, 2023, **452**, 139496.

157 S. Li, T. Jiang, H. Zhang, Y. Li, Q. Cheng, H. Kang, Y.-N. Jing, L. Xiao, X. Zhang, G. Lu, Y. Zhang and H. Zhou, *Sol. RRL*, 2023, **7**, 2201011.

158 Y. Sun, L. Nian, Y. Kan, Y. Ren, Z. Chen, L. Zhu, M. Zhang, H. Yin, H. Xu, J. Li, X. Hao, F. Liu, K. Gao and Y. Li, *Joule*, 2022, **6**, 2835–2848.

159 B. Fan, W. Zhong, W. Gao, H. Fu, F. R. Lin, R. W. Y. Wong, M. Liu, C. Zhu, C. Wang, H.-L. Yip, F. Liu and A. K. Y. Jen, *Adv. Mater.*, 2023, **35**, 2302861.

160 M. Ghasemi, L. Ye, Q. Zhang, L. Yan, J.-H. Kim, O. Awartani, W. You, A. Gadisa and H. Ade, *Adv. Mater.*, 2017, **29**, 1604603.

161 J. Huang, H. Wang, K. Yan, X. Zhang, H. Chen, C.-Z. Li and J. Yu, *Adv. Mater.*, 2017, **29**, 1606729.

162 F. J. M. Colberts, M. M. Wienk, R. Heuvel, W. Li, V. M. Le Corre, L. J. A. Koster and R. A. J. Janssen, *Adv. Energy Mater.*, 2018, **8**, 1802197.

163 Y. Wang, X. Wang, B. Lin, Z. Bi, X. Zhou, H. B. Naveed, K. Zhou, H. Yan, Z. Tang and W. Ma, *Adv. Energy Mater.*, 2020, **10**, 2000826.

164 H.-W. Cheng, A. Mohapatra, Y.-M. Chang, C.-Y. Liao, Y.-T. Hsiao, C.-H. Chen, Y.-C. Lin, S.-Y. Huang, B. Chang, Y. Yang, C.-W. Chu and K.-H. Wei, *ACS Appl. Mater. Interfaces*, 2021, **13**, 27227–27236.

165 Z. J. S. Li, Q. Ma, Y. Wu, Q. Meng, J. Zhang, B. Qiu, J. Qiao and Y. Li, *Sol. RRL*, 2022, **6**, 2200496.

166 S. Li, C. Shi, X. Luo, D. Li, X. Lu, Y. Hu, J. Yuan and Y. Zou, *Sol. RRL*, 2023, **7**, 2201090.

167 F. Zhao, C. Wang and X. Zhan, *Adv. Energy Mater.*, 2018, **8**, 1703147.

168 R. S. Gurney, D. G. Lidzey and T. Wang, *Rep. Prog. Phys.*, 2019, **82**, 036601.

169 J. Hou, O. Inganäs, R. H. Friend and F. Gao, *Nat. Mater.*, 2018, **17**, 119–128.

170 K. Zhou, Y. Wu, Y. Liu, X. Zhou, L. Zhang and W. Ma, *ACS Energy Lett.*, 2019, **4**, 1057.

171 Y. Xu, J. Yuan, S. Liang, J.-D. Chen, Y. Xia, B. W. Larson, Y. Wang, G. M. Su, Y. Zhang, C. Cui, M. Wang, H. Zhao and W. Ma, *ACS Energy Lett.*, 2019, **4**, 2277–2286.

172 S. Liang, Z. Lou, Q. Zhang, Y. Xu, F. Jin, J. Yuan, C. Sheng, W. Ma and H. Zhao, *J. Phys. Chem. C*, 2020, **124**, 25262–25269.

173 T. Shan, Y. Hong, L. Zhu, X. Wang, Y. Zhang, K. Ding, F. Liu, C.-C. Chen and H. Zhong, *ACS Appl. Mater. Interfaces*, 2019, **11**, 42438–42446.

174 H. Fu, Z. Peng, Q. Fan, F. R. Lin, F. Qi, Y. Ran, Z. Wu, B. Fan, K. Jiang, H. Y. Woo, G. Lu, H. Ade and A. K. Y. Jen, *Adv. Mater.*, 2022, **34**, 2202608.

175 W. Xu, X. Zhu, X. Ma, H. Zhou, X. Li, S. Y. Jeong, H. Y. Woo, Z. Zhou, Q. Sun and F. Zhang, *J. Mater. Chem. A*, 2022, **10**, 13492–13499.

176 Y. Zhang, B. Wu, Y. He, W. Deng, J. Li, J. Li, N. Qiao, Y. Xing, X. Yuan, N. Li, C. J. Brabec, H. Wu, G. Lu, C. Duan, F. Huang and Y. Cao, *Nano Energy*, 2022, **93**, 106858.

177 Q. Wu, W. Wang, Y. Wu, Z. Chen, J. Guo, R. Sun, J. Guo, Y. Yang and J. Min, *Adv. Funct. Mater.*, 2021, **31**, 2010411.

178 D. Zhou, C. Liao, S. Peng, X. Xu, Y. Guo, J. Xia, H. Meng, L. Yu, R. Li and Q. Peng, *Adv. Sci.*, 2022, **9**, 2202022.

179 X. Yang, R. Sun, Y. Wang, M. Chen, X. Xia, X. Lu, G. Lu and J. Min, *Adv. Mater.*, 2022, **35**, 2209350.

180 C. Zhao, J. Yi, L. Wang, G. Lu, H. Huang, H. K. Kim, H. Yu, C. Xie, P. You, G. Lu, M. Qiu, H. Yan, S. Li and G. Zhang, *Nano Energy*, 2022, **104**, 107872.

181 C. Cao, H. Wang, D. Qiu, T. Zhao, Y. Zhu, X. Lai, M. Pu, Y. Li, H. Li, H. Chen and F. He, *Adv. Funct. Mater.*, 2022, **32**, 2201828.

182 B. Li, X. Zhang, Z. Wu, J. Yang, B. Liu, Q. Liao, J. Wang, K. Feng, R. Chen, H. Y. Woo, F. Ye, L. Niu, X. Guo and H. Sun, *Sci. China: Chem.*, 2022, **65**, 1157–1163.

183 C. Zhao, L. Wang, G. Zhang, Y. Wang, R. Hu, H. Huang, M. Qiu, S. Li and G. Zhang, *Molecules*, 2022, **27**, 5739.

184 K. Khandelwal, S. Biswas, A. Mishra and G. D. Sharma, *J. Mater. Chem. C*, 2022, **10**, 13–43.

185 Y. Song, K. Zhang, S. Dong, R. Xia, F. Huang and Y. Cao, *ACS Appl. Mater. Interfaces*, 2020, **12**, 18473–18481.

186 P. Xue, J. Xin, G. Lu, B. Jia, H. Lu, G. Lu, W. Ma, R. P. S. Han and X. Zhan, *J. Mater. Chem. C*, 2023, **11**, 8121–8128.

187 H.-C. Wang, P. Cheng, S. Tan, C.-H. Chen, B. Chang, C.-S. Tsao, L.-Y. Chen, C.-A. Hsieh, Y.-C. Lin, H.-W. Cheng, Y. Yang and K.-H. Wei, *Adv. Energy Mater.*, 2021, **11**, 2003576.

188 D. Yang, R. Zhang, Y. Shi, X. Guo and M. Zhang, *J. Mater. Chem. C*, 2022, **10**, 14597–14604.

189 X. Huang, Y. Cheng, Y. Fang, L. Zhang, X. Hu, S. Y. Jeong, H. Zhang, H. Y. Woo, F. Wu and L. Chen, *Energy Environ. Sci.*, 2022, **15**, 4776–4788.

190 C. Xu, K. Jin, Z. Xiao, Z. Zhao, Y. Yan, X. Zhu, X. Li, Z. Zhou, S. Y. Jeong, L. Ding, H. Y. Woo, G. Yuan and F. Zhang, *Sol. RRL*, 2022, **6**, 2200308.

191 M. Bates, C. Malhado, C. Yang, C. K. Herrera and R. R. Lunt, *Sol. RRL*, 2023, **7**, 2200962.

192 L. Duan and A. Uddin, *Adv. Sci.*, 2020, **7**, 1903259.

193 H. K. H. Lee, A. M. Telford, J. A. Röhr, M. F. Wyatt, B. Rice, J. Wu, A. de Castro Maciel, S. M. Tuladhar, E. Speller, J. McGettrick, J. R. Searle, S. Pont, T. Watson, T. Kirchartz, J. R. Durrant, W. C. Tsoi, J. Nelson and Z. Li, *Energy Environ. Sci.*, 2018, **11**, 417–428.

194 M. O. Reese, A. M. Nardes, B. L. Rupert, R. E. Larsen, D. C. Olson, M. T. Lloyd, S. E. Shaheen, D. S. Ginley,

G. Rumbles and N. Kopidakis, *Adv. Funct. Mater.*, 2010, **20**, 3476–3483.

195 S. Dong, K. Zhang, B. Xie, J. Xiao, H.-L. Yip, H. Yan, F. Huang and Y. Cao, *Adv. Energy Mater.*, 2019, **9**, 1802832.

196 R. Sun, J. Guo, Q. Wu, Z. Zhang, W. Yang, J. Guo, M. Shi, Y. Zhang, S. Kahmann, L. Ye, X. Jiao, M. A. Loi, Q. Shen, H. Ade, W. Tang, C. J. Brabec and J. Min, *Energy Environ. Sci.*, 2019, **12**, 3118–3132.

197 K. Y. Ryu, J. Lee, T. Jun, D. Lee, B. Kim, D. Y. Ryu and K. Kim, *ACS Appl. Mater. Interfaces*, 2022, **14**, 23474–23486.

198 M. Hong, J. Youn, K. Y. Ryu, S. Shafian and K. Kim, *ACS Appl. Mater. Interfaces*, 2023, **15**, 20151–20158.